AN INVESTIGATION OF WARM SEASON CO TRANSPORT EPISODES DURING INTEX-A USING SYNTHETIC MOPITT RETRIEVALS

Christopher M. Kiley,[1]
Henry E. Fuelberg,[1]
Louisa Emmons,[2]
John Gille,[2]
Debbie Mao,[2]
Youhua Tang,[3]
Gregory Carmichael[3]

[1]Department of Meteorology, Florida State University, Tallahassee
[2]National Center for Atmospheric Research, Boulder, Colorado
[3]Center for Global & Regional Environmental Research, University of Iowa, Iowa City, Iowa

Submitted to

Journal of Geophysical Research
INTEX-A Special Section

August 2006

ABSTRACT

Pollution and its transport are global problems that require space-derived measurements for diagnosis and research. Since carbon monoxide (CO) has a median lifetime of approximately two months, it is a good tracer of tropospheric circulations. This study determines the extent to which space-based MOPITT retrievals describe CO during several meteorological scenarios. Our procedure creates synthetic MOPITT retrievals using output from the STEM chemical transport model. That is, STEM-derived CO vertical profiles are imported into a radiative transfer code. The calculated radiation spectra then are input to the MOPITT CO retrieval algorithm to create a synthetic version of MOPITT CO. MOPITT is assumed to be in geostationary orbit, and the effects of clouds are not considered. Simulated imagery is shown to be a valuable tool for understanding the capabilities of current sensors and the potential for new sensors to be placed on different platforms. This type of study would not have been possible using operational retrievals.

We examine three phenomena observed during INTEX-A: Alaskan fires, urban plumes, and a warm conveyor belt. The evolution of thick, broad STEM CO patterns in the mid-troposphere is well represented by the synthetic MOPITT CO retrievals. Due to the MOPITT retrievals having coarse vertical resolution, as well as being constrained by a priori information, differences in the magnitudes of STEM and MOPITT CO were often seen. Neglecting differences in magnitude, MOPITT is shown to be useful at describing CO during several meteorological scenarios, specifically in the upper troposphere.

1. Introduction

Pollution and its transport are global problems that require space-based measurements for diagnosis and research. Carbon monoxide (CO) is a major pollutant that has received considerable attention in the literature. CO is not a direct greenhouse gas because it does not strongly absorb terrestrial infrared energy. However, tropospheric CO represents an important component of the anthropogenic impact on the atmosphere. For example, the oxidation of CO and hydrocarbons in the presence of NO_x is the main mechanism for tropospheric ozone production [*Khalil*, 1995].

More than half of the CO emissions today are man-made. Thus, greatest CO concentrations generally occur near areas of large human population. And, on a global scale, the more densely populated northern hemisphere contains approximately twice as much CO as the southern hemisphere [*Intergovernmental Panel on Climate Change (IPCC*), 2001]. Biomass burning and fossil fuel use are the main sources of man-made CO emissions.

CO has a large range of source strengths and a highly variable distribution. With a median lifetime of approximately 2 months, CO is a good tracer of tropospheric circulations. It has the potential to reveal how chemical species are transported in the troposphere as well as provide information about tropospheric chemical reactions. Since CO mostly is produced and generally is most concentrated in the atmospheric boundary layer, with much smaller concentrations in the stratosphere, it is a potentially useful tracer for studying convective influences and tropospheric/stratospheric exchange [*Pan et al.*, 1998].

Realizing the importance of documenting global CO concentrations, NASA in 1981 launched the Measurement of Atmospheric Pollution from Space (MAPS) gas filter radiometer onboard the Space Shuttle [*Reichle Jr. et al.*, 1982]. MAPS provided the first global view of CO.

Subsequent MAPS missions documented the expected seasonal variations and highlighted the previously underestimated biomass burning regions in Indonesia and Asia [*Christopher et al*., 1998; *Connors et al*., 1999; *Newell et al*., 1999; *Reichle Jr. et al*., 1999]. However, due to MAPS' small nadir only field-of-view (FOV), an entire space shuttle mission of seven to ten days was required to produce a single spatially contiguous global map.

In the late 1980s the measurement of CO profiles was identified as being of primary importance for improving our understanding of the global chemical system. This was recognized by the Eos Science Steering Committee [*Eos,* 1987] and the World Meteorological Organization [*WMO,* 1985].

The first satellite-borne CO sensor, the Measurement of Pollution In The Troposphere (MOPITT) instrument, was launched in 1999 on NASA's Terra satellite. MOPITT uses technology similar to MAPS, i.e., correlation gas filter radiometers, to remotely measure CO in the middle troposphere [*Pan et al*., 1998; *Deeter*, 2003]. However, MOPITT was designed to provide much greater spatial and temporal coverage than was possible from the shuttle platform. Also, unlike MAPS, MOPITT includes multiple spectrally distinct channels which permit retrieval of CO's vertical distribution. Nonetheless, approximately three days still are required to construct a composite contiguous map of tropospheric CO. The six-year archive of MOPITT data has contributed to studies of biomass burning regions and inverse modeling to assess emissions inventories [e.g., *Menard et al*., 2002; *Heald*, 2003; *Lamarque et al*., 2003; *Pfister et al*., 2005]. MOPITT-derived CO data are utilized in this current study.

The next generation satellite-borne CO sensor, the Atmospheric InfraRed Sounder (AIRS), was launched in 2002 onboard NASA's Aqua satellite. The AIRS view from Aqua covers approximately 70-85% of the planet between 60^{o}N and 60^{o}S on a daily basis, typically

seeing more than 50% of the United States each day [*Aumann et al*., 2003]. These additional CO retrievals enable process studies of phenomena occurring on daily time scales. Currently, however, AIRS CO retrievals are run only in a research mode.

Several sources of pollution and its transport have received considerable attention. Biomass burning releases large amounts of gases and particles into the atmosphere. These emissions are thought to significantly influence the Earth's atmosphere and climate [*Pickering et al*., 1996]. Although previously it was thought that biomass burning primarily took place over tropical continents [*Crutzen and Andreae*, 1990], satellite remote sensing has shown that biomass burning occurs throughout the globe, including the United States [*Roy et al*., 2002; *Simon et al*., 2002].

A second important topic is the intercontinental transport of pollution [e.g., *Martin et al*., 2003; *Parrish and Law*, 2004]. The major mechanisms for transferring pollution from the planetary boundary layer (PBL) to the free troposphere (FT) include lifting by warm conveyor belts (WCBs) associated with mid-latitude cyclones [e.g., *Stohl,* 2001; *Liu et al*., 2003; *Kiley et al.,* 2006] and lifting by convection [e.g., *Jacob et al*., 1993; *Liu et al*., 2003; *Duncan and Bey*, 2004].

Extratropical wave cyclones are thought to be the dominant mode of tropospheric trace gas transport in the mid-latitudes [*Cotton et al*., 1995; *Donnell et al*., 2001; *Stohl*, 2001]. A greater understanding of cyclone related transport is needed since polluted boundary layer air lifted to higher altitudes can perturb natural chemical concentrations, impact the global radiation budget, and affect air quality at distant locations downstream.

Convective updrafts quickly carry pollutants from the lower atmosphere into the middle and upper troposphere where the stronger horizontal winds lead to rapid transport to distant

locations. Over industrialized continents, convection leads to efficient export of pollutants into the free troposphere [*Lin et al*., 2004]. Convection also has been shown to play a major role in exporting large amounts of pollutants from biomass burning [*Pickering et al*., 1996, *Chatfield et al*., 1996].

The major objective of this study is to illustrate the ability of MOPITT CO retrievals to capture various pollution transport mechanisms. This objective is pursued by synthesizing MOPITT CO retrievals from CO simulated by a chemical transport model (CTM) for three scenarios of interest: Alaskan fires, urban plumes, and WCBs.

2. Data and Methodology

2.1 INTEX-A

NASA's Intercontinental Chemical Transport Experiment (INTEX-A) aircraft campaign [*Singh et al*., 2006], a component of the International Consortium of Atmospheric Research on Transport and Transformation (ICARTT) [Fehenseld et al., 2006], was conducted between June and August 2004. The numerous instrument, chemical transport modeling, and satellite retrieval groups participating in the campaign provided a unique opportunity to understand the mechanisms by which pollution is lofted and transported during the warm season.

2.2 Terra Spacecraft and MOPITT Instrument

NASA launched the Earth Observing System (EOS) Terra satellite during December 1999. Terra's polar orbit is sun synchronous at an altitude of 705 km, with an approximate 10:30 local equator-crossing time.

The MOPITT instrument [*Drummond*, 1996] onboard Terra is an infrared gas correlation radiometer designed to measure tropospheric CO and methane. MOPITT is a downward looking, cross-track scanning instrument, designed to make fourteen measurement steps on either

side of nadir. MOPITT's horizontal resolution at nadir is 22 x 22 km, with cross-track scanning covering a swath 640 km wide. This cross-track scanning allows near global coverage in approximately 3 days. All results to be discussed here are from the version 3 MOPITT CO retrieval algorithm [*Deeter et al.*, 2003].

2.3 Creating a Synthetic Set of CO Retrievals

Validation of satellite-derived measurements usually is performed with aircraft-derived data or sondes; however, these often are limited by their sparse data coverage. CTMs with their underlying meteorology provide unique opportunities to diagnose and understand pollution transport mechanisms seen by the satellite in 3-D space over a large area. The main purpose of the current study is to determine the extent to which MOPITT retrievals capture CO influenced by various meteorological conditions. Thus, CTM-derived CO vertical profiles in areas of interest are imported into forward radiative transfer code to calculate radiation spectra. The calculated radiation spectra then are input to the MOPITT CO retrieval code to create a synthetic version of MOPITT CO. As a result of the above steps, the synthetic MOPITT retrievals are fully consistent with the underlying meteorology of the CTM. Thus, the CTM and its known meteorology provide a link between the synthetic CO distribution and the processes that produced it. The following sections provide details on how these synthetic CO retrievals were created.

2.4 Chemical Transport Model

Global and regional CTMs are valuable tools for quantifying the impact of intercontinental pollution transport on the global distribution of key chemical species. They are fast becoming standard tools for improving our knowledge of chemical budgets and processes in the troposphere. They also are used to provide chemical forecasts for field programs [*Flatoy et*

al., 2000; *Hudman et al*., 2004; *Wang et al*., 2004], to provide a priori information for satellite retrievals [*Palmer et al*., 2001], to examine aerosol-chemistry-climate interactions [*Adams et al*., 2001], and to guide international environmental policy assessments [*IPCC*, 2001].

Current global CTMs provide a horizontal resolution ranging from 1.5^{o} to 4^{o} (~ 150 to 400 km), with a vertical spacing of 50 to 100 m within the boundary layer, 500 to 1000 m in the middle/upper troposphere, and 1200-1500 m near the tropopause [*Wild et al*., 2003]. Without adequate parameterization schemes, the processes involved in lifting trace compounds out of the PBL often are not well represented with this resolution [*Donnell et al*., 2001; *Kiley et al*., 2003].

A limited number of regional scale CTMs have been developed to better resolve small scale processes [*Carmichael et al*., 1986; 1990; 2002; 2003a; *Hess*, 2000; *Vukicevic and Hess*, 2000; *Uno et al*., 2003]. The meteorological quantities used by these regional scale CTMs are provided by mesoscale models.

The Sulfur Transport Eulerian Model (STEM) regional CTM [*Carmichael et al*., 1986, 1990, 2002, 2003a, 2003b] is the high quality model [*Kiley et al*., 2003] used in this study. STEM was developed to investigate relationships between emissions, atmospheric transport, chemical transformation, removal processes, and the resulting distribution of air pollutants and deposition patterns on meso and regional scales. Starting from emissions inventories (area and point sources), meteorology (wind, temperature, humidity, precipitation, etc.), and a set of chemical initial and boundary conditions, STEM simulates pollutant behavior in the selected domain.

For this study, STEM was run at a horizontal resolution of 60 x 60 km, with 21 vertical sigma levels. Meteorological data for STEM were provided by the Fifth-Generation Mesoscale Model (MM5) described in the next section. Advection was calculated using the Galerkin

scheme [*McRae et al*., 1982]. STEM employs a chemical mechanism tool, the kinetic preprocessor for chemical mechanism (KPP), to determine chemical reactions. STEM uses the SAPRC99 chemical mechanism [Carter, 2000] and the second-order Rosenbrock method for dispersion [*Verwer et al*., 1997]. Initial and boundary conditions are specified with the Model of Ozone and Related Tracers (MOZART) simulations during Summer 2004 [*Pfister et al.*, 2005].

2.5 Meteorological Data

The MM5 was used to generate three hourly meteorological data for the STEM model. MM5 is a nonhydrostatic, primitive equation model that is described by *Anthes and Warner* [1978], *Dudhia* [1993], and *Grell et al*. [1994].

The model domain was centered over the continental United States. The grid had 60 km horizontal separation and utilized 21 vertical sigma levels. Nine of these levels were below 850 hPa to provide enhanced vertical resolution at low altitudes. Model components included the Medium Range Forecast (MRF) planetary boundary layer scheme [*Hong and Pan*, 1996], the Grell cumulus parameterization scheme [*Grell et al*., 1994], and a simple ice microphysical scheme to represent saturated processes.

Initial and lateral boundary conditions for the MM5 were obtained from three-dimensional (3-D) global final (FNL) analyses prepared by the National Center for Environmental Prediction (NCEP) and available from the National Center for Atmospheric Research (NCAR). These data were at 6 h intervals and 1.0° horizontal resolution. Four-dimensional data assimilation (FDDA) was employed to relax the model simulations toward the synoptic analyses, thus facilitating the correct placement of features of interest and effectively reducing model error growth [*Stauffer and Seaman*, 1990; *Stauffer et al*., 1991; *Stauffer and Seaman*, 1994; *Seaman and Michelson*, 2000].

2.6 Radiative Transfer Algorithm

The MOPITT operational fast radiative transfer model (MOPFAS) relies on radiative parameterizations to avoid time-consuming spectral integrations [*Edwards et al*., 1999]. A regression technique similar to the optical path transmittance regression scheme (OPTRAN) [*McMillan et al*., 1995] establishes a correspondence between channel-integrated transmittances and atmospheric state profiles. The regression maps a set of predictors, obtained from the state profiles, onto corresponding values of channel transmittance obtained from the MOPITT absorption (MOPABS) model with line-by-line accuracy. The regression coefficients are precomputed as a least-squares fit over a representative atmospheric ensemble. MOPFAS computed radiances typically agree with line-by-line calculations to within 1%, but are approximately 2 orders of magnitude faster to compute [*Edwards et al*., 1999].

Both MOPFAS and MOPABS include contributions from H_2O, CO_2, O_3, N_2O, CO, and CH_4. Required inputs are the vertical distributions of these species as well as atmospheric temperature, surface temperature, emissivity, and reflectivity. Profiles of CO_2, O_3, and N_2O currently are from climatological data sets. Meteorological data were from the MM5. The 4.7 μm thermal emissivity distribution over the globe was determined from the *Fu and Liou* [1992] radiative transfer model parameters that are assigned to each U.S. Geological Survey scene type [*Belward and Loveland*, 1996], as described by *Wilber et al.* [1999].

2.7 MOPITT CO Retrieval Algorithm

The problem of inverting a set of measured radiances to determine aspects of the atmospheric state often is ill-conditioned, meaning there is no unique solution [*Rodgers et al*., 2000]. Thus, additional information usually is required to constrain the retrieval within physically reasonable limits. The CO retrieval algorithm used for MOPITT exploits the

maximum a posteriori (MAP) solution which is a specific type of optimal estimation technique [*Rodgers*, 2000; *Pan et al*., 1998]. The general strategy of such techniques is to seek the solution that is most statistically consistent with both the measured radiances and the typical observed patterns of CO vertical profiles as represented by the a priori. It is important to note that the a priori CO profile for this study is identical to that used by the operational MOPITT retrievals. Details about the mathematical formulation for the MOPITT CO retrieval algorithm are given by *Deeter et al*. [2003].

MOPITT CO concentrations are reported at seven vertical levels (surface, 850, 700, 500, 300, 250, and 150 hPa) and as a total column. However, these data levels do not represent eight independent pieces of information. The information content in MOPITT CO profiles can be objectively quantified using Degrees of Freedom for Signal (DFS). DFS values greater than one, indicating some profile shape information, are common in tropical and mid-latitude scenes [*Deeter et al*., 2004]. In general, MOPITT retrieves two layers approximately corresponding to the mid- and upper-troposphere (i.e., centered on 700 and 350 hPa). Thus, we will only discuss MOPITT retrievals at these two levels.

The overall goal of this study was to determine the extent to which MOPITT retrievals capture CO influenced by various meteorological conditions. Therefore, several assumptions were made. First, standard operational MOPITT CO retrievals are performed only in cloud-free pixels. The presence of clouds is determined by comparing the retrieved surface temperature to NCEP analyzed surface temperatures, along with the Moderate Resolution Imaging Spectroradiometer (MODIS) cloud mask product [*Warner et al*., 2001]. However, we did not include clouds in our study since 3-D STEM-derived CO, which was imported to the forward radiative transfer algorithm, was available at each grid point throughout the period. This

idealized approach permits the comparison of MOPITT and STEM CO in cloudy regions where operational MOPITT CO retrievals would not be performed, i.e., near cyclones, convection, fronts, and other meteorological features of interest.

Another interesting aspect of this study is that MOPITT was assumed to be onboard a geostationary satellite. Thus, retrievals are calculated at each grid point of the model domain, without considering the actual location of the MOPITT instrument. Treating MOPITT as geostationary and neglecting clouds allows comparisons with STEM at all locations within our model domain at all times during INTEX-A. Finally, it should be noted that geostationary satellites have a greater field-of-view than polar orbiters due to their higher altitudes. However, for this study we assumed that MOPITT's FOV does not change between polar and geostationary frames of reference.

To resemble real-time MOPITT CO retrievals, prescribed noise was added to the radiance values. Standard values of instrument noise (Mnoise) and forward model uncertainty (Fnoise) were used (Ben Ho, personal communication). Depending on the spectral channel (i), values of Mnoise ranged from 3.84e-13 to 1.03e-11 W m^{-2} Sr^{-1}, while Fnoise ranged from 6.88e-11 to 1.94e-08 W m^{-2} Sr^{-1}. Random noise with Gaussian statistics was calculated as:

$$\text{Noise}(i) = \text{rand} * [(\text{Mnoise}(i))^2 + (\text{Fnoise}(i))^2]^{1/2} \qquad (1)$$

where rand is a random number between 0 and 1. This random noise is added to each channel's radiance value.

3. Results

STEM-derived CO was examined each day during INTEX-A to locate interesting spatial patterns. Three scenarios of interest, Alaskan fires, urban plumes, and a warm season warm conveyor belt (WCB), were selected for further study because they represented important phenomena during INTEX-A. In particular, pollution from Alaskan fires and urban plumes were the two main ingredients comprising INTEX-A WCBs.

Synthetic MOPITT CO retrievals based on STEM CO profiles and MM5 meteorological data were created at 3 h intervals during three periods. This procedure allowed us to examine the usefulness of MOPITT CO retrievals to diagnose pollution episodes and transport mechanisms.

3.1 Alaskan Fires Case

The 2004 Alaskan summer was unusual [*Fuelberg et al*., 2006; *Richmond and Shy*, 2005; *Turquety et al*., 2006]. The anomalous weather led to a record-breaking 6.5 million acres being burned [*ADEC*, 2004]. Beginning in May, a deep cut-off upper low persisted over the Gulf of Alaska, while a strong ridge with positive height anomalies covered northern Alaska and northwest Canada (Figure 1a). This left Alaska under a prevailing easterly low to mid level flow. Adequate moisture and weak short-wave disturbances provided the focus for organized deep convection where abundant lightning ignited a multitude of wildfires. In late June, an anomalously strong upper-level ridge built over northern, and then northwestern Alaska (Figure 1b). The fires grew explosively during this long period of warm, dry conditions. During much of July, thick smoke from the large wildfires shrouded the entire Fairbanks area. Atypical for the month was the fact that no low pressure systems penetrated the prevailing ridge pattern from the southwest or west. Widespread convection and rainfall that typically develop by the end of July would have slowed, or even ended, the large-scale active fire growth. However during 2004, the

dry pattern continued through August, often the wettest month for Alaska, allowing the wildfires to continue. CO distributions throughout the INTEX-A period were significantly impacted by these anomalous conditions.

Greatest upper level STEM CO concentrations during INTEX-A occurred on 26 July 2004. To locate the source of this upper level enhancement, we used the Hazard Mapping System (HMS) fire and smoke product [*Prins et al*., 2001]. HMS is an interactive processing system that allows trained satellite analysts in NOAA's Satellite Analysis Branch (SAB) to manually integrate data from various automated fire detection algorithms using GOES data and several polar imaging sources (Advanced Very High Resolution Radiometer (AVHRR), Moderate Resolution Imaging Spectroradiometer (MODIS) Fire Algorithm, and Defense Meteorological Satellite Program/Operational Linescan System (DMSP/OLS)). The result is a quality controlled display of fire locations and significant smoke plumes. Locations of fires and smoke plumes during 26-29 July 2004 are shown in Figure 2. Widespread fires are located throughout much of Alaska and northwest Canada. Transport from the fires is clearly indicated by the HMS product and by *Damoah et al*. [2005] and *Fuelberg et al.* [2006] using backward trajectories. The smoke plumes impacted much of the United States, reaching as far south as Oklahoma and Tennessee.

The reader is reminded that MOPITT generally retrieves two layers approximately corresponding to the mid- and upper-troposphere; thus, we will only discuss MOPITT retrievals at 700 and 350 hPa. However, we do not limit our view of STEM CO to these two layers in an effort to identify the most interesting CO features.

STEM-derived CO between 26-29 July 2004 reveals the influence of the Alaskan fires (Figure 3a). As stated previously, greatest upper level STEM CO concentrations during INTEX-

A occurred on 26 July 2004 when values at 600 hPa exceeded 350 ppbv. This enhancement is due to the Alaskan fires as evidenced by trajectories (not shown) and its location within a major smoke plume (Figure 2a). Interesting spatial patterns in STEM CO also are evident during the period. MM5 forecasts of 500 hPa steamlines are shown in Figure 4. A trough located just west of the Great Lakes on 26 July (Figure 4a) produces northwesterly flow out of Canada. The next day, a closed low pressure area develops in the region (Figure 4b) causing the CO plume to split. One portion of the plume remains at northern latitudes where it is rapidly transported by the westerly jet stream. The other portion travels southward due to interaction with the low pressure area. This southward moving branch eventually reaches the Gulf Coast on 29 July before further progression is impeded by the Bermuda High.

The synthetic MOPITT CO retrievals at 700 hPa for the 26-29 July 2004 period are shown in Figure 3b. These retrievals include the assumed noise described earlier. The horizontal evolution of the STEM CO spatial patterns is well represented by the synthetic MOPITT retrievals. In particular, MOPITT identifies the split CO pattern on 27 July, the location of the low pressure center, and the counterclockwise transport wrapping around its base on 28 July. However, the southward branch of MOPITT CO does not extend as far south as STEM which shows enhanced CO extending over the Gulf of Mexico (Figure 3a). In general, however, the MOPITT fields show a good capability for representing the upper level horizontal transport of CO, even in complex situations.

Figure 3c shows the operational MOPITT CO retrievals for this same period, 26-29 July. The Alaskan fire plume is apparent in these images; however, the satellite swath pattern and the clouds accompanying the low pressure system significantly limit the picture of CO transport. The

benefit of increased spatial coverage provided by the assumed geostationary platform for the synthetic MOPITT retrievals is clearly evident.

We next examine vertical distributions of CO at four individual pixels on 27 July 2004 (Figure 5). These pixels span the large mid-tropospheric plume at about 40°N (across Nebraska and Iowa). The left panels contain the original STEM CO model input, the a priori CO, and the simulated MOPITT retrieval. The right column of Figure 5 shows averaging kernels for each retrieval level. The averaging kernels describe the relative weighting between the true and a priori profiles. Thus, the averaging kernels, along with the a priori profile, can be used to transform the true or model profile to be directly comparable to the MOPITT retrievals. The averaging kernels also give an indication of the vertical resolution of the retrievals.

Similar to *Emmons et al.* [2004], the current synthetic MOPITT profiles can be expressed as transformations of the STEM and a priori profile (x_a):

$$\text{MOPITT} = A * \text{STEM} + (I-A)* x_a, \qquad (2)$$

where A is the averaging kernel matrix and I is the identity matrix [*Rodgers*, 2000]. Thus, each MOPITT retrieval is equal to the total profile times the averaging kernel for that level, plus (one minus the averaging kernel) times the a priori profile.

Each of the four STEM vertical profiles (Figure 5) exhibits the large enhancement of mid-tropospheric CO due to the Alaskan wildfires that were seen on 27 July in Figure 3. However, the MOPITT vertical profiles cannot resolve the vertical structure of this layer. For example, MOPITT CO is greater than STEM CO and the a priori below 700 hPa. This low level enhancement is a result of MOPITT smoothing the enhanced CO throughout the vertical column. In plan view (Figure 3), the evolution of spatial STEM CO patterns is well represented by the synthetic MOPITT CO imagery. The color scale in Figure 3 was chosen because it is ideal for

highlighting the evolution of patterns; however, it is important to note that the magnitude of MOPITT CO in the plumes is ~ 150 ppb less than that of STEM. These differences between the STEM and synthetic MOPITT retrievals in mid-troposphere plumes are due to the coarse vertical resolution of MOPITT.

MOPITT currently uses a single a priori profile. Alaskan fires were responsible for anomalously high CO during Summer 2004, and their effect is not contained in the a priori. If a CTM such as STEM were used to create a first guess field that varied spatially, the retrievals undoubtedly would be improved. Such a procedure would be similar to that used to retrieve profiles of temperature and humidity from meteorological satellites [e.g., Fuelberg and Olson, 1991]. That is, spatially varying profiles from a numerical meteorological model serve as the first guess which then is refined by the satellite's radiances.

3.2 Urban Plumes Case

The widespread mid and upper tropospheric CO enhancement due to the Alaskan fires often made it difficult to distinguish between fire induced CO and low level urban CO plumes. Figure 6a shows CO concentrations simulated by STEM at 850 hPa for the 2-5 August 2004 period. This frequently occurring INTEX-A pattern exhibits enhanced STEM CO from the Alaskan fires being transported toward the Gulf and Atlantic Coasts in the low levels (Figure 6a). An examination of three hourly STEM CO images (not shown) reveals urban pollution from the Washington DC and New York City areas mixing with CO from the Alaskan fires on 2-3 August. A surface cold front then sweeps through the eastern United States on 4 August, transporting the large CO concentrations offshore. This plume began over the cities and now has moved out over the ocean. The synthetic MOPITT CO retrievals (Figure 6b) detect and correctly place the urban plume off the northeast coast. Once again, however, magnitudes of MOPITT CO

are much weaker than those of STEM. In particular, MOPITT CO is ~ 100 ppbv smaller than STEM throughout the plume. Vertical profiles near New York City (Figure 7) reveal that the plume remains below 500 hPa. The MOPITT retrievals do not provide adequate information at low altitudes for detecting the magnitude of this CO plume, as illustrated by the averaging kernels (Figure 7, right panels). However, MOPITT's values below ~ 700 hPa are intermediate to those of the a priori and STEM, showing enhanced CO in the lower troposphere.

The influence of Alaskan fires began to subside over the eastern United States during mid August. Figure 8a shows STEM CO concentrations at four levels on 9 August 2004. This case provides an ideal study of urban plumes since upper tropospheric CO concentrations are relatively small (50 to 85 ppbv) over the large eastern urban areas at 350 and 500 hPa, allowing us to examine MOPITT's response to low altitude CO plumes. In the lowest levels (850 hPa), STEM reveals CO enhancement over much of the southeast United States. However, STEM reveals greater enhanced CO concentrations associated with major metropolitan areas, such as Atlanta, Chicago, Cleveland, Dallas, Detroit, Houston, New York City, and Washington, DC. We hypothesized that the MOPITT CO retrievals would exhibit only minimal response to the low level urban CO plumes. However, individual MOPITT pixels do appear to indicate some enhanced CO near Atlanta, Cleveland, Dallas, Detroit, and Washington, DC. Individual profiles near New York, Washington, Atlanta and Houston are shown in Figure 9. The STEM CO profiles in this case are of sufficient magnitude through a thick enough layer near the surface to show somewhat enhanced values in the MOPITT 700 hPa retrievals. However most of the pollution layer is at altitudes where the averaging kernels are quite weak. Thus, MOPITT appears to provide some information about the location of low level urban pollution in this case.

However, due to the lack of sensitivity of the retrievals to concentrations in the boundary layer, this is generally not the case.

3.3 Warm Season Warm Conveyor Belt Case

The WCB is a warm moist flow that ascends from the boundary layer and lower troposphere ahead of the surface cold front of a mid-latitude cyclone [*Carlson*, 1998]. During INTEX-A, pollution from Alaskan fires and urban areas often mixed together along the East Coast (Figure 6). This well mixed, highly polluted air then was lofted from low to mid levels by synoptic scale cyclones and their associated WCBs.

Kiley and Fuelberg [2006] studied WCBs during INTEX-A. They found that the causes for and locations of maximum vertical transport within WCBs display large case-to-case variability. In particular, they identified convection south and southwest of a mid latitude cyclone's center as the dominant mechanism producing vertical transport during the warm season INTEX-A period when large scale baroclinic pressures were weak. A cyclone on 19 July 2004 illustrated their findings. We now determine which features of this WCB are distinguishable in MOPITT CO retrievals. The MM5 configuration that was used with STEM is somewhat different from that of *Kiley and Fuelberg* [2006]. Key differences include vertical resolution, convective parameterization schemes, initial and lateral boundary conditions, and output intervals. However, these differences are not important to the current study since STEM CO only is compared with its synthetic counterpart, and not with actual measurements.

The coherent ensemble of trajectories (CET) technique [*Wernli and Davies*, 1997; *Wernli*, 1997] was used to identify WCBs. A grid of kinematic trajectories was launched from 900 hPa and calculated forward in time for 48 h. A complete description of our trajectory model can be found in *Fuelberg et al*. [1996, 1999, 2000] and *Martin et al*. [2002]. The current CET

criteria for defining a WCB are identical to *Kiley and Fuelberg* [2006], i.e., ascent of at least 5000 m, a potential temperature increase of 15 K, and a specific humidity decrease of 10 g kg^{-1} are required within 48 h. Figure 10 shows the 48 h CET begun at 0600 UTC 21 July 2004. This starting time, two days after *Kiley and Fuelberg* [2006], was chosen because of its more interesting CO patterns. Figure 10 shows two features that meet the WCB criteria. The first, WCB 1, is located over the Atlantic Ocean with a starting point just east of Florida. WCB 1 corresponds to the 19 July 2004 episode described by *Kiley and Fuelberg* [2006]. Consistent with the frequent frontal passages during INTEX-A [*Fuelberg et al*., 2006], the second CET feature, WCB 2, is located over the central United States. Both CETs exhibit southerly flow that ascends over time.

The distribution of CO on 21 July is shown in Figure 11. STEM CO (Figure 11a) shows three elongated features at most pressure levels. Specifically, a prominent STEM CO feature corresponding to WCB 1 (Figure 10) is observed at 350 hPa over the Atlantic Ocean (Figure 11a). The swirl near its southern end, east of Florida, represents interaction with a tropical cyclone. The second elongated STEM feature, which is best defined at and below 500 hPa (Figure 11a), straddles the Eastern Seaboard. Interestingly, this CO elongation does not meet the CET criteria used to describe a WCB (Figure 10). The third elongated STEM CO feature, but defined at 500 hPa, is located further west, stretching from the Appalachians into Canada (Figure 11a). It corresponds to WCB 2 (Figure 10). Although the second STEM CO feature does not meet our trajectory based WCB criteria, it is interesting to examine using MOPITT imagery.

Synthetic MOPITT CO resembles STEM CO at the highest levels. At 350 hPa (Figure 11b) MOPITT reproduces several aspects of the STEM spatial patterns. The prominent CO feature corresponding to WCB 1 over the Atlantic is especially interesting. The synthetic

MOPITT retrievals clearly identify the shape and magnitude of this enhanced CO region north of 35° N. However, south of 35° N, MOPITT is unable to capture the correct CO magnitude, and the cyclonic pattern is not distinguishable (Figure 11). An examination of vertical profiles (not shown) reveals that the northern portion of WCB 1 is a strong and thick plume; however, it is much thinner further south. The coarse vertical resolution of MOPITT limits its ability to identify the thin plume.

The broad elongated STEM CO enhancement (the combination of features two and three at 350 hPa) is not well documented by MOPITT (Figure 11). Instead, MOPITT CO patterns at 350 hPa (Figure 11b), appear more similar to STEM CO at 500 hPa than to STEM CO patterns at 350 hPa. As an example, one should note the broad band of STEM CO at 350 hPa along the eastern seaboard (Figure 11a). MOPITT captures the magnitude of STEM CO at 350 hPa (Figure 11b); however, it shows less skill at representing the spatial patterns. MOPITT splits the broad plume at 350 hPa into two elongated features. In particular, MOPITT depicts a narrow band of CO extending along the Gulf Coast near 30° N to just off the New England coast. A more western elongated CO feature also is revealed by MOPITT at 350 hPa. Thus, the 500 hPa CO appears to dominate the vertical column in this scenario. In this case, the MOPITT retrievals are sensitive to the CO distribution near 500 hPa and therefore do not capture the vertical structure of this enhancement.

MOPITT exhibits considerably less ability to reproduce STEM's spatial features in the lower troposphere. At 700 hPa (Figure 11b), MOPITT CO patterns appear more similar to STEM CO at 500 hPa and 850 hPa (Figure 11a) than to STEM CO patterns at 700 hPa (Figure 11a). As an example, one should note the southwestward oriented CO feature at 500 hPa extending through Pennsylvania, New York, and Canada (Figure 11a). This feature is not seen at

850 hPa in the STEM imagery; however, it is seen by MOPITT at 700 hPa (Figure 11b). Once again, the MOPITT retrievals are sensitive to the upper level CO, causing the upper troposphere to dominate the MOPITT CO pattern in the lower levels. As a second example, the magnitude of the CO feature over the Atlantic Ocean, corresponding to WCB 1, is 100 ppbv greater in MOPITT than in STEM, due to the influence of the a priori in the MOPITT retrievals. The westernmost STEM CO feature is shaped similar to a "v" north of the Great Lakes at 850 hPa; however, MOPITT only identifies the eastern side of the "v". However, one should note that the 850 hPa averaging kernels peak at 700 hPa, showing the close relationships between those levels. To summarize, low level MOPITT CO retrievals do not provide sufficient information to identify WCB-like features (Figure 11).

We next examine the usefulness of MOPITT vertical profiles in identifying WCB transport mechanisms. Three vertical profiles were strategically selected along the elongated CO feature straddling the East Coast (Figure 12). This MOPITT image at 700 hPa is an enhanced version of the one in Fig 11b. The STEM CO vertical profiles at these locations (Figure 13) identify the fundamental characteristics of a WCB. The bottom row (32° N) shows low level pollution entering the WCB near the Gulf Coast. The middle row (34.6° N) shows pollution being transported northward and lofted to 500 hPa near coastal North Carolina. The top row (42.2° N) displays an interesting profile near Cape Cod. The small enhancement near 500 hPa appears to represent the continued evolution of pollution transport through the WCB as it is exhausted over the Atlantic. In addition, enhanced CO, apparently from the Northeast Corridor, dominates the lower levels of the profile. This scenario represents the mixing of low level urban pollution into the ascending northward moving airstream. Thus, the STEM CO feature has

characteristics of a WCB even though it did not meet the WCB criteria in the CET analysis (Figure 10).

The MOPITT vertical profiles (Figure 13) reveal a very different scenario from STEM. On 21 July 2004 the magnitudes of all three synthetic MOPITT CO features (Figure 11b) in the middle troposphere are considerably smaller than those from STEM, similar to Figure 3. Once again, this bias is explained by the coarse vertical resolution and the influence of the a priori profile on the retrieval. Similar to Figure 5, the MOPITT vertical profiles (Figure 13) show virtually no enhancement that identifies the vertical transport of CO by the apparent WCB; CO merely decreases with height. Generally speaking, the MOPITT retrievals are unable to resolve the magnitude and vertical characteristics of CO within this WCB-like feature.

3.4 Possible Next Generation CO Remote Sensor

Section 2 discussed two major assumptions in this study. First, we treated MOPITT as though it were onboard a geostationary satellite. To our knowledge, this is the first time that MOPITT CO retrievals have been presented in this reference frame. Second, clouds were not included in our study. These two assumptions allowed synthetic MOPITT CO retrievals to be compared to STEM CO at all times and locations during INTEX-A.

The geostationary assumption permitted the horizontal evolution of CO patterns to be clearly displayed because complete domain coverage was provided at each time step. Conversely, when MOPITT is housed on a polar platform as currently occurs, 3 to 5 days of observations are required for global coverage. To illustrate this point, Figure 3c shows the operational polar orbiting MOPITT CO retrieval for 26-29 July 2004. The enhanced spatial coverage that is provided by a geostationary platform is clearly evident when comparing Figure 3c to Figures 3b and 5. The white areas within swaths are due to clouds (e.g., between 40° and

47° N off of the east coast). However, even if the effects of clouds are neglected, the narrow swaths of the current observations do not reveal the low pressure center (Figure 4) near the Great Lakes.

These results suggest ways to improve current CO remote sensing techniques. Ideally, such an instrument should be housed onboard a geostationary satellite. This configuration would provide unprecedented spatial coverage. The new geostationary instrument would not replace current polar capabilities, but rather supplement them. For example, the global distribution and transport of CO still would be provided by MOPITT aboard Terra, while a geostationary instrument would provide enhanced spatial and temporal coverage over a specific region, much like GOES meteorological satellites complement the polar orbiters.

Although the benefit of a geostationary CO remote sensor is clear, its cost cannot be ignored. A less expensive alternative might provide results that are superior to those currently available. Specifically, an instrument having a larger swath width placed aboard a polar orbiting satellite in low earth orbit would expand the spatial domain, and provide global coverage on a daily or near daily basis. These ideas should be considered when developing the next generation CO remote sensing instrument.

4. Conclusions

The major objective of this study was to determine the usefulness of MOPITT CO retrievals to diagnose and understand pollution transport mechanisms. STEM model simulated CO was examined each day during INTEX-A to locate interesting spatial patterns. Three scenarios of interest, Alaskan fires, urban plumes, and a warm season warm conveyor belt (WCB) were investigated. These episodes were frequent occurrences during INTEX-A.

Synthetic MOPITT CO imagery based on STEM CO profiles and MM5 meteorological data were created for the selected periods. This procedure directly linked the modeled meteorology and chemical information to the simulated CO, allowing us to examine the usefulness of the MOPITT CO imagery to diagnose pollution episodes and transport mechanisms. Simulated imagery was shown to be a valuable tool for understanding the capabilities of current sensors and the potential for new sensors to be placed on different platforms. This type of study would not have been possible using operational retrievals.

Greatest upper level STEM CO concentrations during INTEX-A occurred on 26 July 2004 as a direct result of the Alaskan fires. The evolution of STEM CO patterns in the mid-troposphere was well represented by the synthetic MOPITT CO retrievals. In particular, MOPITT identified the split transport that developed from interaction with a closed low pressure area. However, a major difference between the magnitudes of STEM and MOPITT CO was identified. Specifically, synthetic MOPITT CO in mid-tropospheric plumes was biased approximately 150 ppb smaller than STEM CO. These differences in magnitude are due to the coarse vertical resolution and the constraints of the a priori CO profile on the MOPITT retrievals. The a priori profile monotonically decreases with height, thus illustrating the limitations of MOPITT retrievals in resolving the vertical characteristics of this thin plume.

MOPITT currently uses a single a priori profile for the globe. This use of a single profile can introduce a bias in the MOPITT retrievals, as evidenced in Figure 5. Alaskan fires were responsible for anomalously high CO during Summer 2004; however, MOPITT's a priori input did not contain this current information. The use of a seasonally and spatially varying a priori would reduce this bias. We hypothesized that the CO retrievals would exhibit only minimal response to low level urban CO plumes. Results showed this hypothesis generally to be true;

however, MOPITT did reveal some low level enhancements over the southeast United States on 9 August. Although CO magnitudes were much weaker than those from STEM, the features were placed correctly and were not an artifact of enhanced upper level CO. Thus, MOPITT appears capable of providing some information about the location of low level pollution. However, when CO levels are enhanced in both the mid-troposphere and near the surface, the MOPITT retrievals cannot resolve the altitude of the pollution.

The warm moist flow that ascends from the boundary layer and lower troposphere ahead of the surface cold front within a WCB was examined. MOPITT CO retrievals resembled a WCB in the upper levels. However, CO retrievals in the lower troposphere did not provide sufficient information to identify the WCB transport. Thus, based on images of constant altitude of MOPITT CO alone, one could easily misidentify the WCB.

This study using synthetic imagery has illustrated the ability of MOPITT retrievals to capture CO distributions in a variety of meteorological conditions. However, one must remember that record-breaking burning occurred during the study period, and MOPITT's a priori did not account for the significant increase in CO over the United States due to these fires. Such an inclusion might have produced much smaller differences in CO magnitude between STEM and MOPITT. Neglecting differences in magnitude, MOPITT was shown to be useful at describing CO during several meteorological scenarios, specifically in the upper troposphere.

Acknowledgements. The authors which to thank the entire MOPITT Science Team, particularly David Edwards, Daniel Ziskin, Ben Ho and Merritt Deeter for their collaboration on this project. This research was sponsored by NASA's Tropospheric Chemistry Program under Grant

NNG04GC33G. The MOPITT Science Team would like to acknowledge the support of NASA's EOS program.

REFERENCES

Adams, P. J., J. H. Seinfeld, D. Koch, L. J. Mickley, and D. J. Jacob, General circulation model assessment of direct radiative forcing by the sulfate-nitrate-ammonium-water inorganic aerosol system*, J. Geophys. Res*., **106**, 1097-1111, 2001.

Alaska Department of Environmental Conservation (DEC), 2004 Wildland Fire Season Summary, http://www.dec.state.ak.us/air/am/2004_wf_sum.htm.

Anthes, R. A., and T. T. Warner, Development of hydrodynamic models suitable for air pollution and other mesometeorological studies, *Mon. Wea. Rev.,* **106**, 1045-1078, 1978.

Aumann, H. H., M. T. Chahine, C. Gautier, M. D. Goldberg, E. Kalnay, L. M. McMillin, H. Revercomb, P. W. Rosenkranz, W. L. Smith, D. H. Staelin, L. L. Strow, and J. Susskind, AIRS/AMSU/HSB on the Aqua mission: Design, science objectives, data products, and processing systems, *IEEE Transactions of Geoscience and Remote Sensing*, **41**, 2003.

Belward A., and T. Loveland, The DIS 1-km land cover data set, IGBP (International Geosphere-Biosphere Project) *NewsLetter 27*, 7-9, 1996.

Carlson, T. N., *Mid-Latitude Weather Systems*, American Meteorological Society, Boston, 1998.

Carmichael, G. R., et al., Evaluating regional emission estimates using the TRACE-P observations, *J. Geophys. Res*., 108(D21), 8810, doi:10.1029/2002JD003116, 2003a.

Carmichael, G. R., et al., Regional-scale chemical transport modeling in support of intensive field experiments: Overview and analysis of the TRACE-P observations, *J. Geophys. Res*., 108(D21), 8823, doi:10.1029/2002/JD003117, 2003b.

Carmichael, G. R., G. Calori, H. Hayami, I. Uno, S. Y. Cho, M. Engardt, S.-B. Kim, Y. Ichikawa, Y. Ikeda, J.-H. Woo, H. Ueda and M. Amann, The MICS-Asia study: Model intercomparison of long range transport and sulfur deposition in East Asia, *Atmos. Environ.,* **36**, 175-199, 2002.

Carmichael, G. R., L. K. Peters and R. D. Saylor, The STEM-II regional scale acid deposition and photochemical oxidant model-I. An overview of model development and applications, *Atmos. Environ.,* **25A**, 2077-2090, 1990.

Carmichael, G. R., L. K. Peters and T. Kitada, A second generation model for regional scale transport / chemistry / deposition, *Atmos. Environ.,* **20**, 173-188, 1986.

Carter, W. P. L., Documentation of the SPARC-99 chemical mechanism for VOC reactivity assessment final report to California Air Resources Board. Technical Report. University of California at Riverside, 2000.

Chatfield, R. B., J. A. Vastano, H. B. Singh, and G. Sachse, A general model of how fire emissions and chemistry produce African/oceanic plumes (O_3, CO, PAN, smoke) in TRACE A, *J. Geophys. Res*., Vol. **101**, D19, 24,279-24,306, 1996.

Christopher, S. A., J. Chou, and R. M. Welch, Satellite investigations of fire, smoke, and carbon monoxide during April 1994 MAPS mission: Case studies over tropical Asia, *J. Geophys*. Res., **103** 19,327-19,336, 1998.

Connors V. S., B. B. Gormsen, S. Nolf, and H. G. Reichle Jr., Spaceborne observations of the global distribution of carbon monoxide in the middle troposphere during April and October 1994, *J. Geophys. Res*., **104**, 21-455-21,470, 1999.

Cotton, W. R., G. D. Alexander, R. Hertenstein, R. L. Walko, R. L. McAnelly, and M. Nicholls, Cloud venting – a review and some new global annual estimates, *Earth-Science Rev., **39***, 169-206, 1995.

Crutzen, P. J. and M. O. Andreae, Biomass burning in the tropics: Impact on atmospheric chemistry and biogeochemical cycles. *Science* 250, 1669-1678, 1990.

Damoah R., et al., Transport modeling of a pyro convection event in Alaska, *Atmos. Chem. and Phys*., 2005.

Deeter, M. N., L. K. Emmons, D. P. Edwards, and J. C. Gille, Vertical resolution and information content of CO profiles retrieved by MOPITT, *Geophys. Res. Lett.,* **31**, doi:10.1029/2004GL020235, 2004.

Deeter, M. N., Operational carbon monoxide retrieval algorithm and selected results for the MOPITT instrument, *J. Geophys. Res*., **108**, doi:10.1029/2002JD003,186, 2003.

Donnell, E. A., D. J. Fish, E. M. Dicks, and A. J. Thorpe, Mechanisms for pollutant transport between the boundary layer and the free troposphere, *J. Geophys. Res*., **106**(D8), 7847-7856, 10.1029/2000JD900730, 2001.

Drummond, J. R., and G. S. Mand, The Measurements of Pollution in the Troposphere (MOPITT) instrument: Overall performance and calibration requirements, *J. Atmos. Ocean Technol*., **13**, 314-320, 1996.

Drummond, J. R., Novel correlation radiometer: The length modulated radiometer, *Appl. Opt*., **28**, 2451-2452, 1989.

Dudhia, J., A nonhydrostatic version of the Penn State/NCAR mesoscale model: Validation tests and simulation of an Atlantic cyclone and cold front, *Mon. Wea. Rev.,* **121**, 1493-1513, 1993.

Duncan, B. N., and I. Bey, A modeling study of export pathways of pollution from Europe: Seasonal and Interannual variations (1987-1997), *J. Geophys. Res*., **109**, DO8301, doi:10.1029/2003JD004079, 2004.

Earth Observing System - Science Steering Committee Report, 1987.

Edwards, D. P., C. M. Halvorson, and J. C. Gille, Radiative transfer modeling for the EOS Terra satellite Measurement of Pollution in the Troposphere (MOPITT) instrument*, J. Geophys. Res*., **104**, 16,755-16,775, 1999.

Emmons, L.K., et al., Validation of Measurements of Pollution in the Troposphere (MOPITT) CO retrievals with aircraft in situ profiles, *J. Geophys. Res., 109(D3)*, D03309, 10.1029/2003JD004101, 2004.

Fehenseld, F. C., et al., International Consortium for Atmospheric Research on Transport and Transformation (ICARTT): North America to Europe: Overview of the 2004 summer field study, J. Geophys. Res., submitted.

Flatoy, F., O. Hov, and H. Schlager, Chemical forecasts used for measurement flight planning during POLINAT 2, *Geophys. Res. Lett*., **27**, 951-954, 2000.

Fu, Q., and K. N. Liou, On the correlated k-distribution method for radiative transfer in nonhomogeneous atmospheres, *J. Atmos. Sci*., **49**, 2139-2156, 1992.

Fuelberg, H. E., M. J. Porter, C. M. Kiley, D. Morse, Meteorological condition and anomalies during INTEX-A, *J. Geophys. Res*., submitted.

Fuelberg, H. E., J. R. Hannan, P. F. J. van Velthoven, E. V. Browell, G. Bieberbach Jr., R. D. Knabb, G. L. Gregory, K. E. Pickering, and H. B. Selkirk, A meteorological overview of the SONEX period. *J.Geophys. Res.,* **105**, 3633-3651, 2000.

Fuelberg, H. E., R. O. Loring Jr., M. V. Watson, M. C. Sinha, K. E. Pickering, A. M. Thompson, G. W. Sachse, D. R. Blake, and M. R. Schoelberl, TRACE-A – A trajectory intercomparison: Part 2. Isentropic and kinematic methods. *J. Geophys. Res.,* **101**, 23927-23939, 1996.

Fuelberg, H. E., and S. R. Olson, An assessment of VAS-derived retrievals and parameters used in thunderstorm forecasting, *Mon. Wea. Rev*., **119**, 795-814, 1991.

Grell, G. A., J. Dudhia, and D. R. Stauffer, A description of the fifth-generation Penn State/MCAR mesoscale model (MM5), *NCAR Technical Note*, NCAR/TN-398+STR, 117 pp., 1994.

Heald, C. L., et al., Asian outflow and trans-Pacific transport of carbon monoxide and ozone pollution: An integrated satellite, aircraft, and model perspective, *J. Geophys*. *Res*., **108**, doi:10.1029/2003JD003,507, 2003.

Hess, P. G., Model and Measurement Analysis of Springtime Transport and Chemistry of the Pacific Basin. *J. Geophys. Res.,* ***106***, D12, 12689-12717, 2000.

Hong, S.-Y., and K.-L Pan, Nonlocal boundary layer vertical diffusion in a medium range forecast model, *Mon. Wea. Rev*., **124**, 2322-2339, 1996.

Horowitz, L., et al., A global simulation of tropospheric ozone and related tracers: Description and evaluation of MOZART, version 2, *J. Geophys. Res*., **108**(D24) 4784, doi:10.1029/2002JD002853, 2003.

Hudman, R. C., D. J. Jacob, O. C. Cooper, M. J. Evans, C. L. Heald, R. J. Park, F. Fehsenfeld, F. Flocke, J. Holloway, G. Hubler, K. Kita, M. Koike, Y. Kondo, A. Neuman, J. Nowak, S. Oltmans, D. Parrish, J. M. Roberts, T. Ryerson, *Ozone production in transpacific Asian pollution plumes and implications for ozone air quality in California*, J. Geophys. Res., 109, D23S10,10.1029/2004JD004974, 2004.

Intergovernmental Panel on Climate Change (IPCC), Atmospheric chemistry and greenhouse gases, *in Climate Change 2001: The Scientific Basis*, edited by J.T. Houghton et al., Cambridge Univ. Press, New York, 2001.

Jacob, D. J., J. A. Logan, G. M. Gardner, R. M. Yevich, C. M. Spivakovsky, S. C. Wosfy, S. Sillman, and M. J. Prater, Factors regulating ozone over the United States and its export to the global atmosphere, *J. Geophys. Res*., **98**:14817, 1993.

Khalil, M. A. K., Decline in Atmospheric Carbon Monoxide Raises Questions About Its Cause, *Earth in Space,* **Vol. 8***,* No. 3, November 1995, p. 7. 1995.

Kiley, C. M. and H. E. Fuleberg, An examination of summertime cyclone transport processes during INTEX-A*, J. Geophys. Res*., in review.

Kiley, C. M., H. E. Fuelberg, P. I. Palmer, D. J. Allen, G. R. Carmichael, D. J. Jacob, C. Mari, R. B. Pierce, K. E. Pickering, Y. Tang, O. Wild, T. D. Fairlie, J. A. Logan, G. W. Sachse, D. G. Streets, 2003: An intercomparison and evaluation of aircraft-derived and simulated CO from seven chemical transport models during the TRACE-P experiment, *J. Geophys. Res.,* **108**(D21), 8819, doi:10.1029/2002JD003089.

Lamarque, J., D. Edwards, L. Emmons, and J. Gille, Identification of CO plumes from MOPITT data: Application to the August 2000 Idaho-Montana forest fires*, J. Geophys. Res*., 2003.

Lin, W. Y., M. H. Zhang, Evaluation of clouds and their radiative effects simulated by the NCAR community atmospheric model against satellite observations. *Journal of Climate*: Vol. 17, No. 17, pp. 3302–3318, 2004.

Liu, H., D. J. Jacob, I. Bey, R. M. Yantosca, B. N. Duncan, and G. W. Sachse, Transport pathways for Asian pollution outflow over the Pacific: Interannual and seasonal variations, *J. Geophys. Res*., **108**(D20), 8786, doi:10.1029/2002JD003102, 2003.

Martin, B. D., H. E. Fuelberg, N. J. Blake, J. H. Crawford, J. A. Logan, D. R. Blake, and G.W. Sachse, Long range transport of Asian outflow to the equatorial Pacific, *J. Geophys. Res*., **108**(D2), 8322, doi:10.1029/2001JD001418, 2003.

McMillan, L. M., L. J. Crone, M. D. Goldberg, and T. J. Kleespies, Atmospheric transmittance of an absorbing gas 4:OPTRAN: A computationally fast and accurate transmittance model for absorbing gases with fixed and variable mixing ratios at variable viewing angles, *Appl. Opt*., vol. **34**, pp. 6269-6274, 1995.

McRae, G. J., W. R. Goodin and J. H. Seinfeld, Numerical solution of the atmospheric diffusion equation for chemical reacting flows, *J. Comput. Phys.,* **45**, 1-42, 1982.

Menard, R. A., Robichaud, and J. Kaminski, Assimiliation and inverse modeling of MOPITT CO observations, in *2002 IEEE International Geoscience and Remote Sensing Symposium* #02CH37380, vol. 2, pp. 1099-1101, 2002.

Newell, R. E., Y. Zhu, V. S. Connors, P. C. Reichle Jr., H. G. Novelli, and B. B. Gormsen, Atmospheric processes influencing measured carbon monoxide in the NASA Measurement of Air Pollution Satellites (MAPS) experiment, *J. Geophys. Res*., **104**(D17), 21,487-21,501, 1999.

Palmer, P. I., D. J. Jacob, K. Chance, R. V. Martin, R. J. D. Spurr, T. P. Kurosu, I. Bey, R. M. Yantosca, A. Fiore, and Q. Li, Air mass factor formulation for spectroscopic measurements from satellites: Application to formaldehyde retrievals from the Global Ozone Monitoring Experiment*, J. Geophys. Res*., **104**, 14,539-14,550, 2001.

Pan, L., J. C. Gille, D. P. Edwards, P. L. Bailey, and C. D. Rodgers, Retrieval of tropospheric carbon monoxide for the MOPITT experiment, *J. Geophys. Res*., **103**, 32,277-32,290, 1998.

Parrish, D., and K. Law, Intercontinental transport and chemical transformation Lagrangian-2k4, IGA *Ctivities Newsletters*, No.**29**, 2003.

Pfister, G., P. G. Hess, L. K. Emmons, J.-F. Lamarque, C. Wiedinmyer, D. P. Edwards, G. Pétron, J. C. Gille, and G. W. Sachse, Quantifying CO emissions from the 2004 Alaskan wildfires using MOPITT CO data, *Geophys. Res. Lett*., **32**, L11809, doi:10.1029/2005GL022995, 2005.

Pickering, K. E., A. M. Thompson, Y. Wang, W.-K. Tao, D. P., McNamara, V. W. J. H Kirchhoff, B. G. Heikes, G. W. Sachse, J. D. Bradshaw, G. L. Gregory, and D. L. Blake, Convective transport of biomass burning emissions over Brazil during TRACE A, *J. Geophys Res*., Vol. **101**, No. D19, 23,993-24,012, 1996.

Prins, E. M., J. Schmetz, L. Flynn, D. Hillger, and J. Feltz, Overview of current and future diurnal active fire monitoring using a suite of international geostationary satellites, *Global and Regional Wildfire Monitoring: Current Status and Future Plans*, F. J. Ahern, J. G. Goldammer, and C. O. Justice, Eds,, SPB Academic, 145-170, 2001.

Reichle Jr., H. G., et al., Space shuttle based global CO measurements during April and October 1994, MAPS instrument, data reduction, and data validation, *J. Geophys. Res*., **104**(D17), 21,443-21,454, 1999.

Reichle Jr., H. G., et al., Carbon monoxide measurements in the troposphere, *Science*, **218**, 1024-1026, 1982.

Richmond, M. A., T. L. Shy, An extraordinary summer in the interior of Alaska, 8th Conference on Polar Meteorology and Oceanography, 2005, Amer. Met. Soc.

Rodgers, C. D., Inverse Methods for Atmospheric Sounding: Theory and Practice, World Scientific, 2000.

Roy, D. P., P. E. Lewis, and C. O. Justice, Burned area mapping using multi-temporal moderate spatial resolution data – a bi-directional reflectance model-based expectation approach, *Remote Sens. Environ*., **83**, 263-286.

Seaman, N. L., and S. A. Michelson, Mesoscale meteorological structure of a high-ozone episode during the 1995 NARSTO-Northeast study, *J. Appl. Meteor.,* **39**, 384-398, 2000.

Simon, S., The ATSR-2 Global Burn Scar Atlas (GLOBSCAR) Project, *Proceedings of the Chemical Weather workshop*, DLR, Munich, Germany, May 7-8, 2002.

Singh, H. B., W. Brune, J. Crawford, and D. Jacob, Overview of the Summer 2004 Intercontinental Chemical Transport Experiment – North America (INTEX-NA), *J. Geophys. Res*., submitted.

Stauffer, D. R., and N. L. Seaman, Use of four-dimensional data assimilation in a limited-area mesoscale model, part I, Experiments with synoptic-scale data, *Mon. Weather Rev.,* **118**, 1250-1277, 1990.

Stauffer, D. R., and N. L. Seaman, Multiscale four-dimensional assimilation, *J. Appl. Meteorol.,* **33**, 416-434, 1994.

Stauffer, D. R., N. L. Seaman, and F. S. Binkowski, Use of four-dimensional data assimilation in a limited area mesoscale model, part II, Effects of data assimilation within the planetary boundary layer, *Mon. Weather Rev.,* 119, 734-754, 1991.

Stohl, A., A 1-year Lagrangian climatology of airstreams in the Northern Hemisphere troposphere and lowermost stratosphere, *J. Geophys. Res*., **106**(D7), 7263-7280, 10.1029/2000JD900570, 2001.

Taylor, F. W., Pressure modulator radiometry, *Spectroscopic Techniques*, G. A. Vanasse, Ed. (Academic, New York, 1983) Vol. 3, pp. 137-197.

Turquety, S., J.A. Logan, D.J. Jacob, R.C. Hudman, F.Y. Leung, C.L. Heald, R. M. Yantosca, S. Wu, L. K. Emmons, D.P. Edwards, and G.W. Sachse, Inventory of boreal fire emissions for North America in 2004: The importance of peat burning and pyro-convective injection, submitted to *J. Geophys. Res.*

Uno, I., et al., Regional chemical weather forecasting system CFORS: Model descriptions and analysis of surface observations at Japanese island stations during the ACE-Asia experiment, *J. Geophys. Res*., **108**(D23), 8668, doi:10.1029/2002JD002845, 2003.

Verwer, J. G., E. J. Spee, J. G. Blom and W. H. Hundsdorfer, A second order Rosenbrock method applied to photochemical dispersion problems. Modelling, Analysis and Simulation (MAS), MAS-R9717, August 31, 1997.

Vukicevic, T., P. Hess, Analysis of tropospheric transport in the Pacific Basin using the adjoint technique. *J. Geophys. Res., 105*, D6, 7213-7230, 2000.

Wang, Y.X., M.B. McElroy, D.J. Jacob, R.M. Yantosca, *A nested grid formulation for chemical transport over Asia: applications to CO*, J. Geophys. Res., 109, D22307, doi:10.1029/2004jd005237, 2004.

Warner, J., J. Gille, D. P. Edwards, D. Ziskin, M. Smith, P. Bailey, and L. Rokke, Cloud detection and clearing for the earth observing system Terra satellite Measurements of Pollution in the Troposphere (MOPITT) experiment, *Appl. Opt*., **40**, 1269-1284, 2001.

Wernli, H., A Lagrangian-based analysis of extratropical cyclones. II: A detailed case study, *Q. J. R., Meteorol, Soc*., **123**, 1677-1706, 1997.

Wernli, H, and H. C. Davies, A Lagrangian-based analysis of Extratropical cyclones. I: The method and some applications, *Q. J. R. Meteorol. Soc*., **123**, 467-489, 1997.

Wilber, A. C., D. P. Kratz, and S. K. Gupta, Surface emissivity maps for use in satellite retrievals of longwave radiation, *NASA Tech. Paper 1999-209362* (NASA Langley Research Center, Hampton, VA.) 1999.

Wild, O., J. Sundet, M. J. Prather, I. Isaksen, H. Akimoto, E. V. Browell, and S. J. Oltmans, CTM ozone simulations for spring 2001 over the western Pacific: Comparisons with TRACE-P lidar, ozonesondes, and TOMS columns, *J. Geophys. Res*., **108**(D21), 8826, doi:10.1029/2002JD003282, 2003.

World Meteorological Organization Report No. 27: WDCGG Data Summary 2003.

World Meteorological Organization Report No. 16: Atmospheric Ozone 1985.

Yu, Z. Z., and J. R. Drummond, A global surface reflectivity data set for the 2.2 – 2.35 μm region, *Int. J. Remote Sens*., **19**, 331-344, 1998.

a)

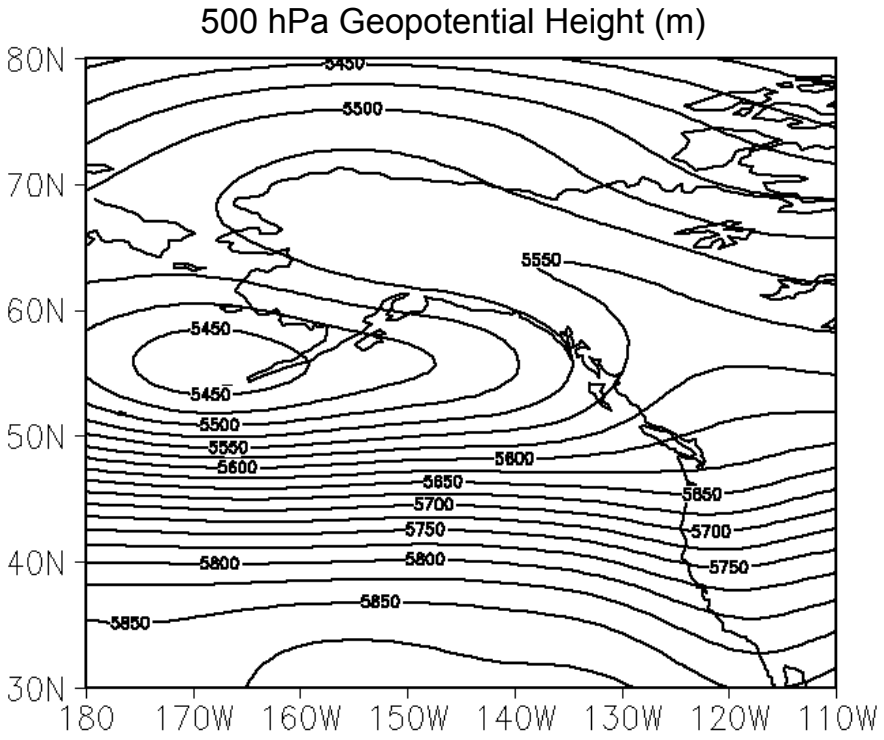

b)

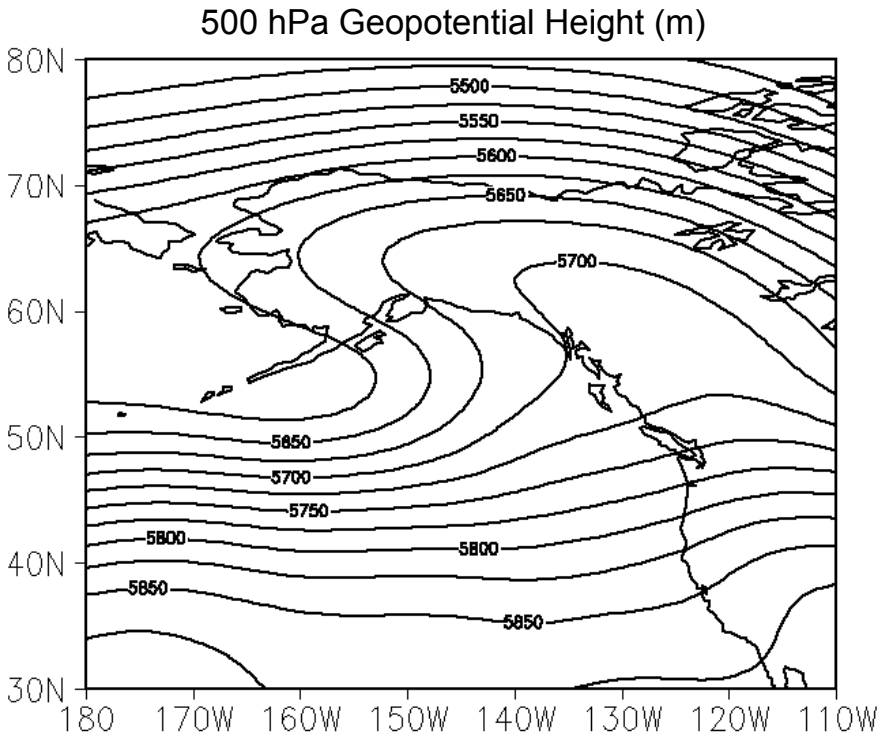

Figure 1. 500 hPa geopotential height composite mean for (a) 30 May – 10 June 2004 and (b) 11 June – 1 August 2004.

Figure 2. HMS fire and smoke product for (a) 26 July 2004, (b) 27 July 2004, (c) 28 July 2004, and (d) 29 July 2004. Fires are black dots, smoke when detected by the analyst, is in grey. See text for details.

a)

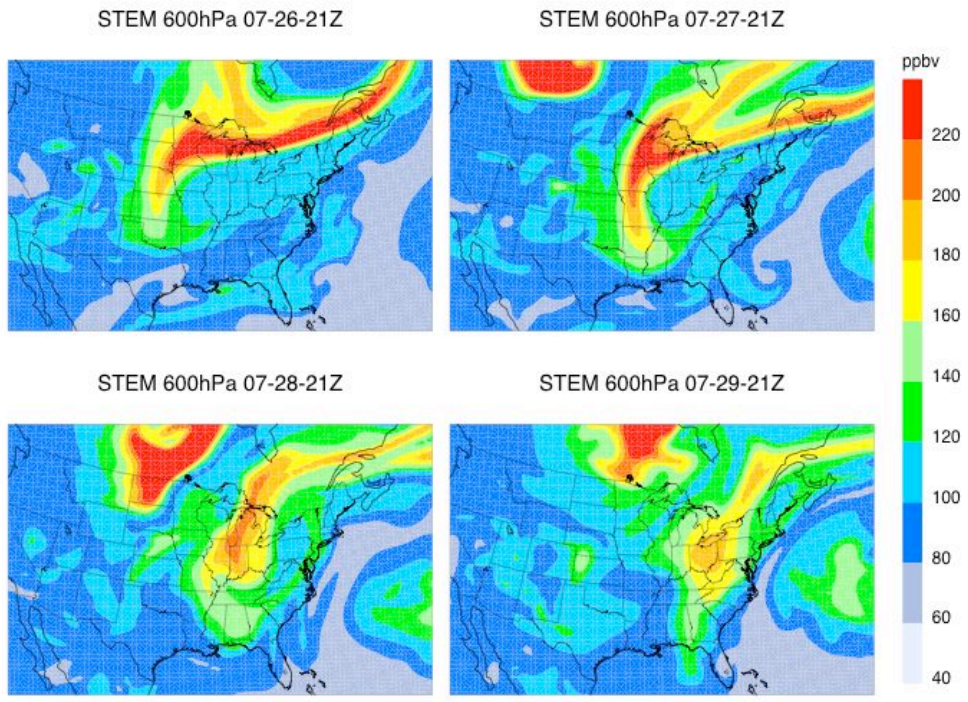

b)

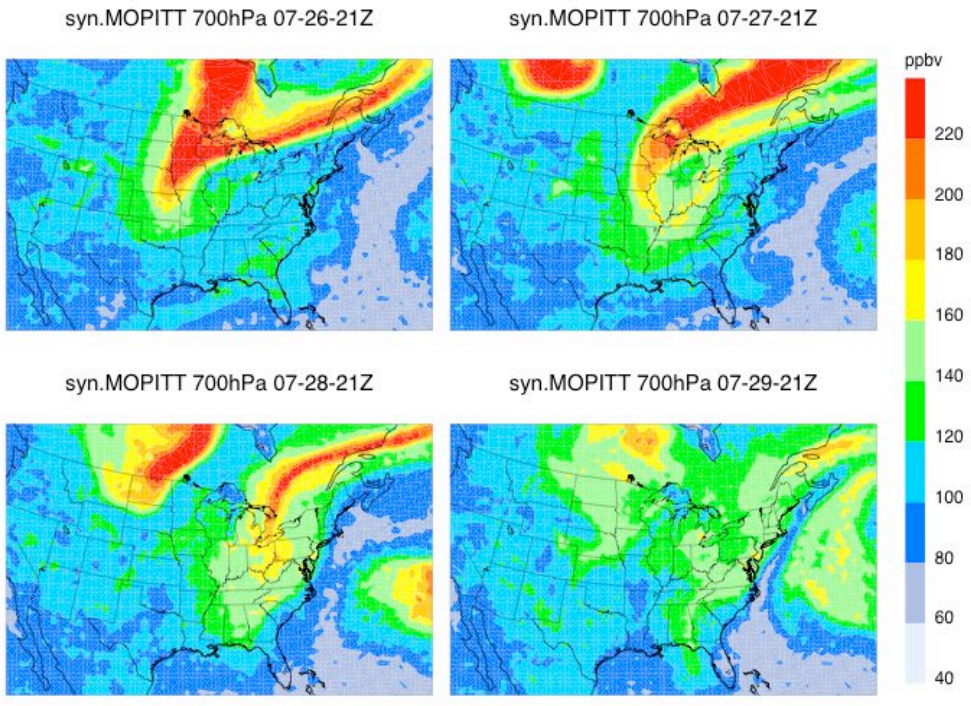

Figure 3. STEM CO and synthetic MOPITT CO distributions for 26-29 July 2004 at 2100 UTC. Top four panels (a): STEM CO (ppbv) at 600 hPa. Bottom four panels (b): synthetic MOPITT CO (ppbv) at 700 hPa.

c)

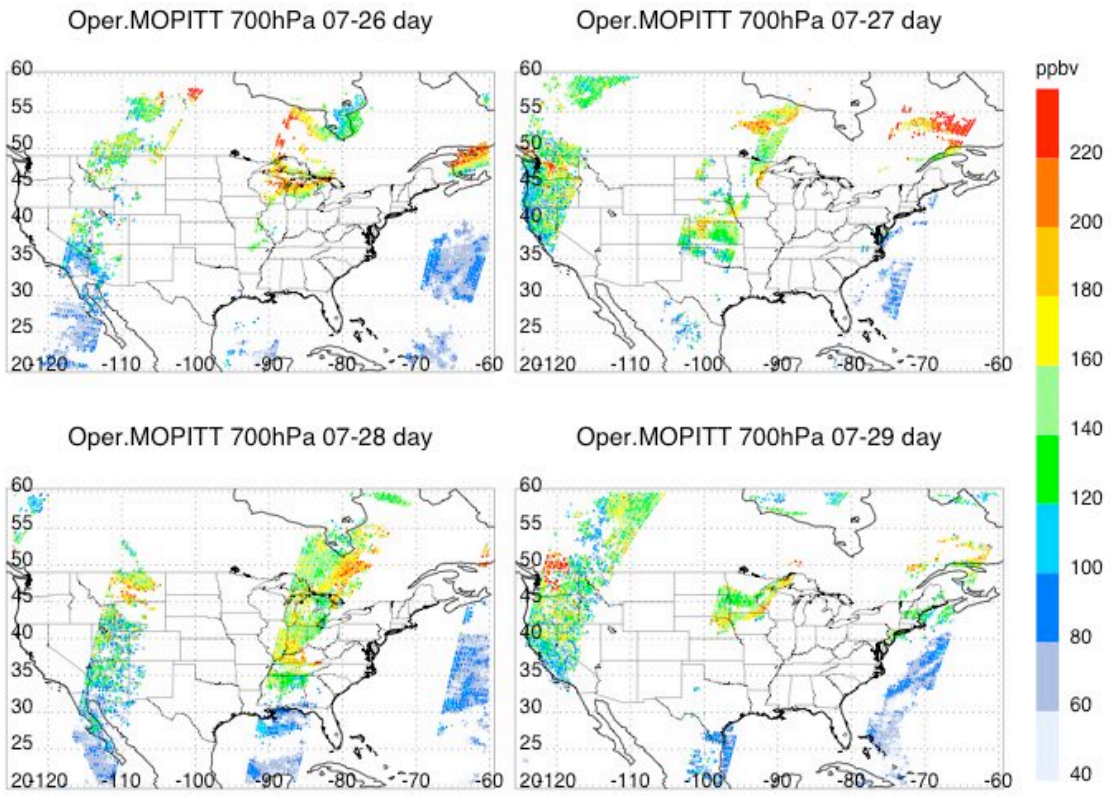

Figure 3 (cont.). (c) Operational MOPITT retrievals for 26-29 July at 700 hPa.

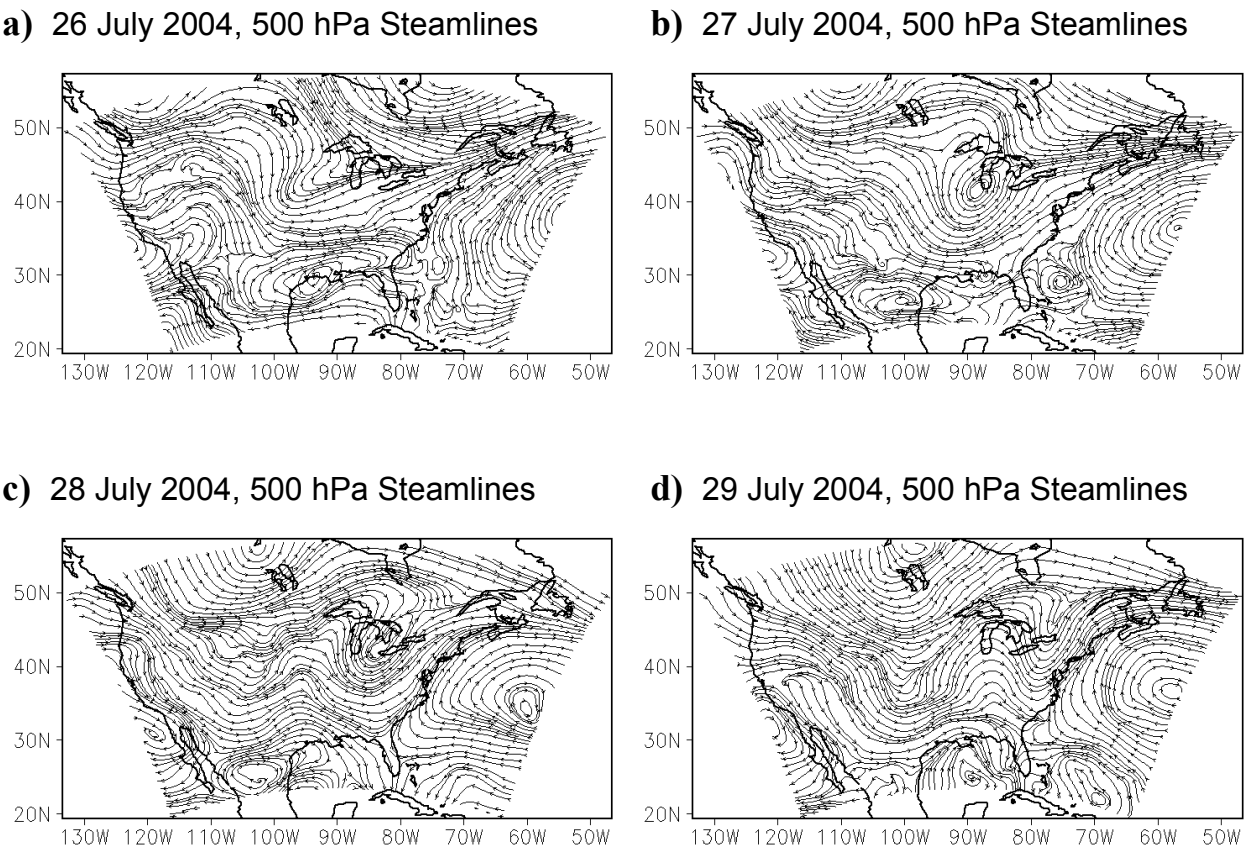

Figure 4. MM5 forecast of 500 hPa steamlines for (a) 26 July 2004, (b) 27 July 2004, (c) 28 July 2004, and (d) 29 July 2004.

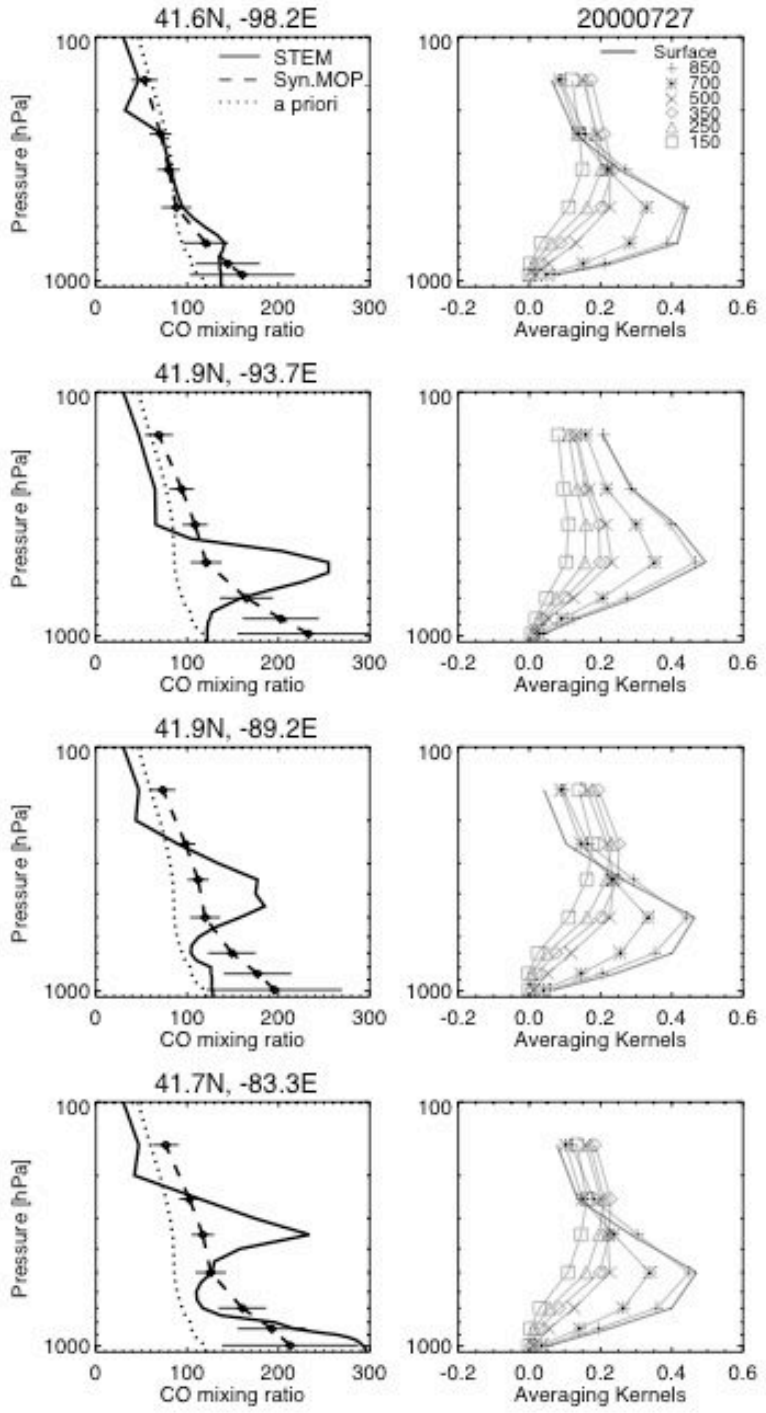

Figure 5. Vertical profiles of CO (ppbv) for several grid boxes/pixels on 27 July 2004 at 2100 UTC. The left panels show the STEM CO profile (solid line), the synthetic MOPITT CO profile (dashed line, with error bars), and the a priori CO profile (dashed, same in each). The right panels show the averaging kernels for each retrieval level (surface to 150 hPa).

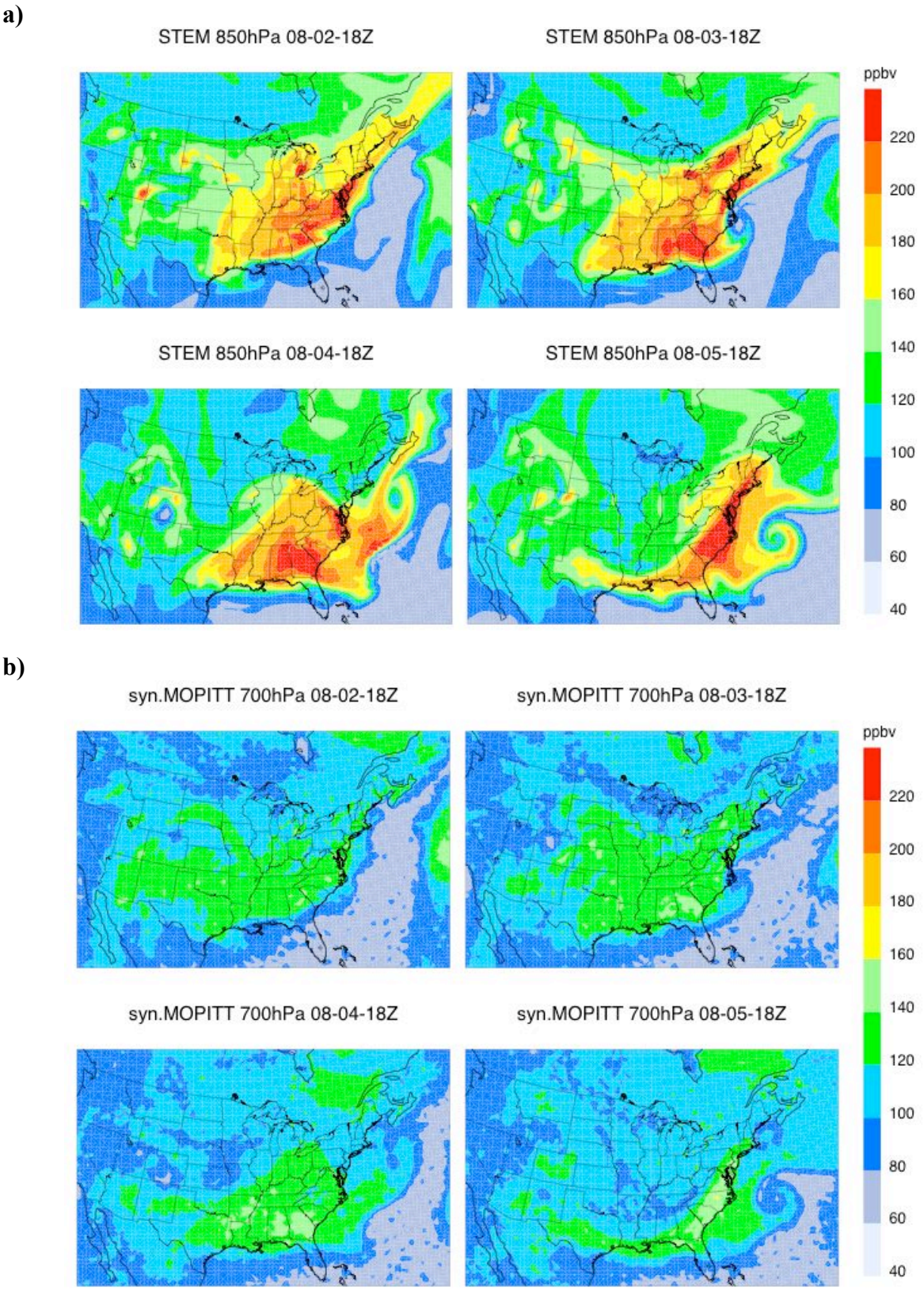

Figure 6. (a) STEM CO (ppbv) at 850 hPa (top four panels) and (b) synthetic MOPITT CO (ppbv) at 700 hPa (bottom four panels) for 2-5 August at 1800 UTC.

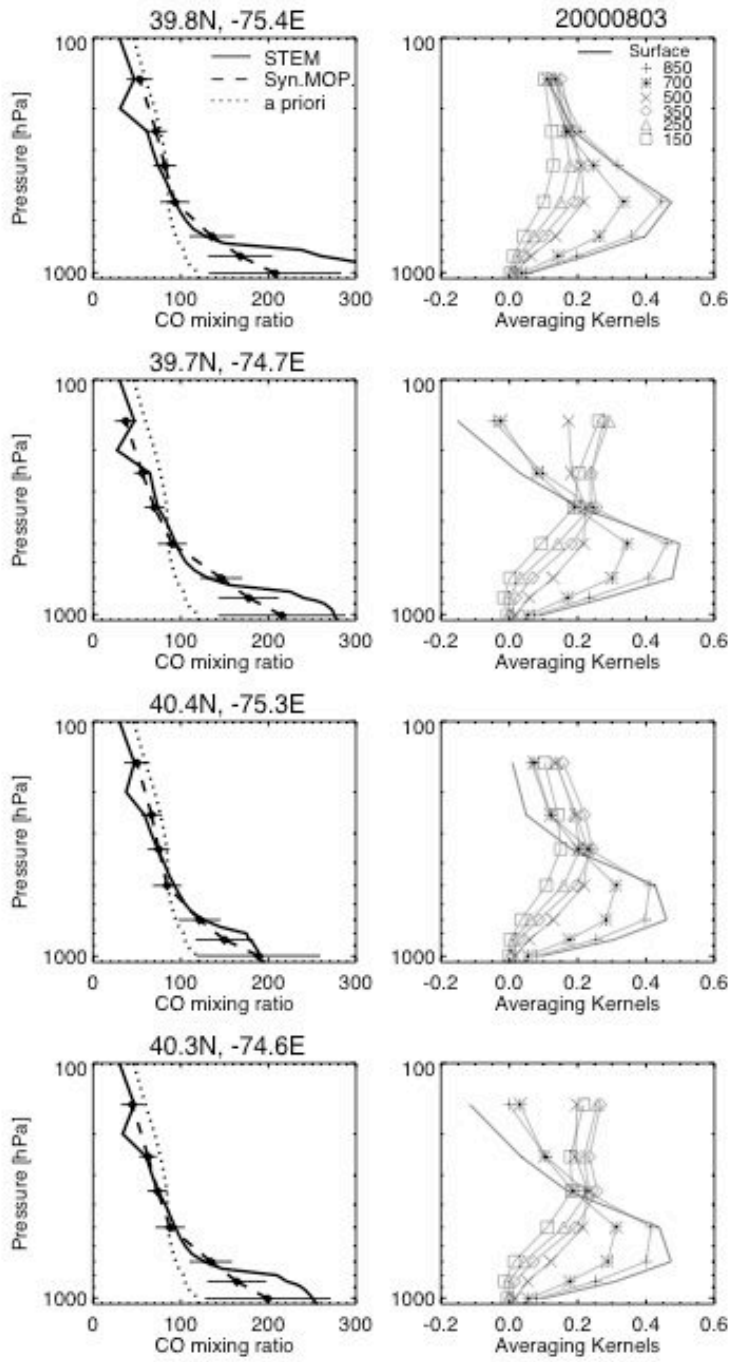

Figure 7. Vertical profiles of CO (ppbv) for 3 August 2004 at 1500 UTC near New York City. The left panels show the STEM CO profile (solid line), the synthetic MOPITT CO profile (dashed line, with error bars), and the a priori CO profile (dashed, same in each). The right panels show the averaging kernels for each retrieval level (surface to 150 hPa).

a)

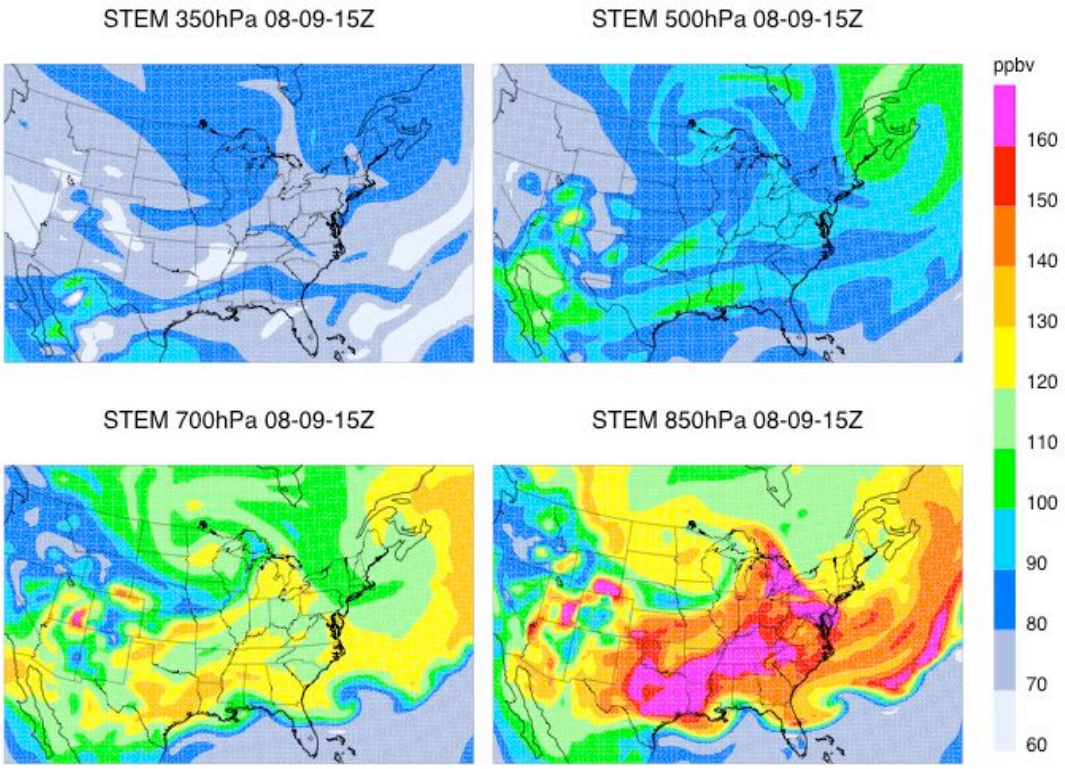

b)

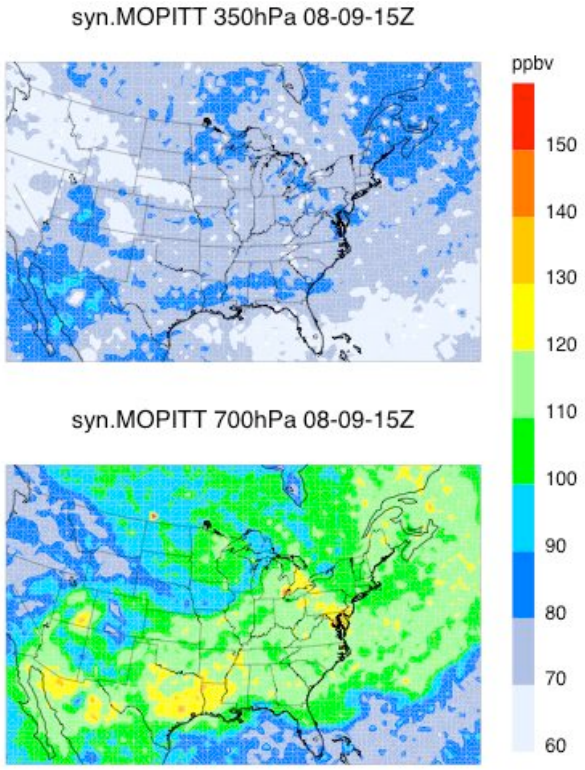

Figure 8. STEM CO (ppbv) and synthetic MOPITT CO (ppbv) for 9 August at 1500 UTC. a) STEM at altitudes 350, 500, 700, and 850 hPa. b) MOPITT at 350 and 700 hPa.

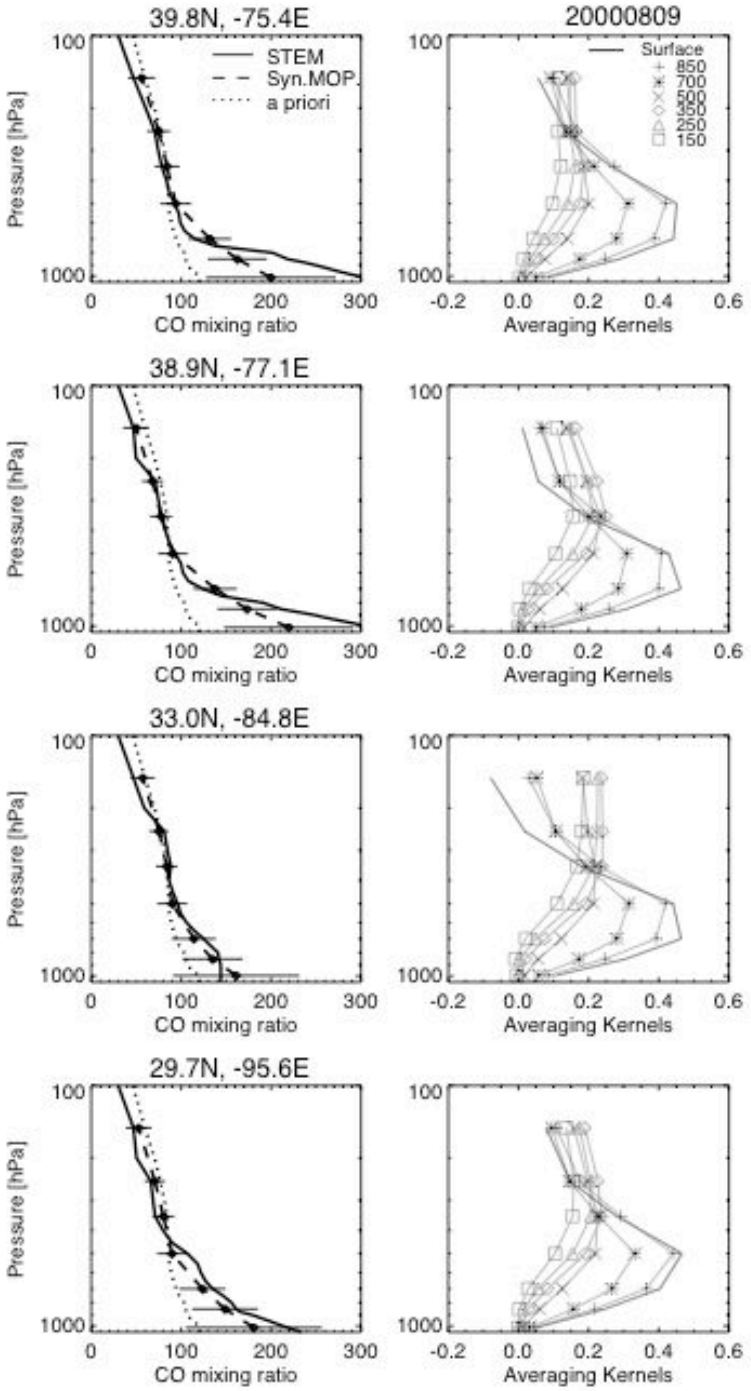

Figure 9. Vertical profiles of CO (ppbv) for 9 August 2004 at 1500 UTC for New York (39.8N, -75.4E), Washington DC (38.9N, -77.1E), Atlanta (33.0N, -84.8E), and Houston (29.7N, -95.6E). The left panels show the STEM CO profile (solid line), the synthetic MOPITT CO profile (dashed line, with error bars), and the a priori CO profile (dashed, same in each). The right panels show the averaging kernels for each retrieval level (surface to 150 hPa).

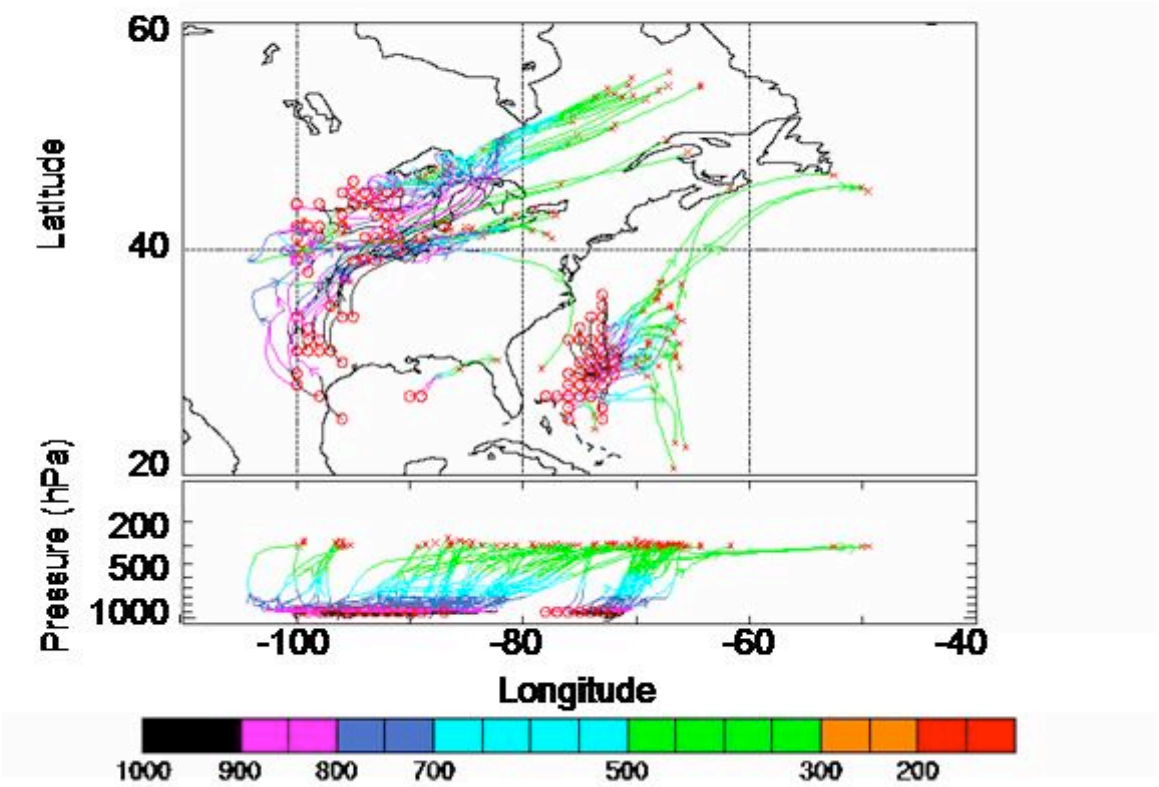

Figure 10. Coherent ensemble of 48 h forward trajectories starting at 900 hPa 21 July 2004 at 0600 UTC.

a)

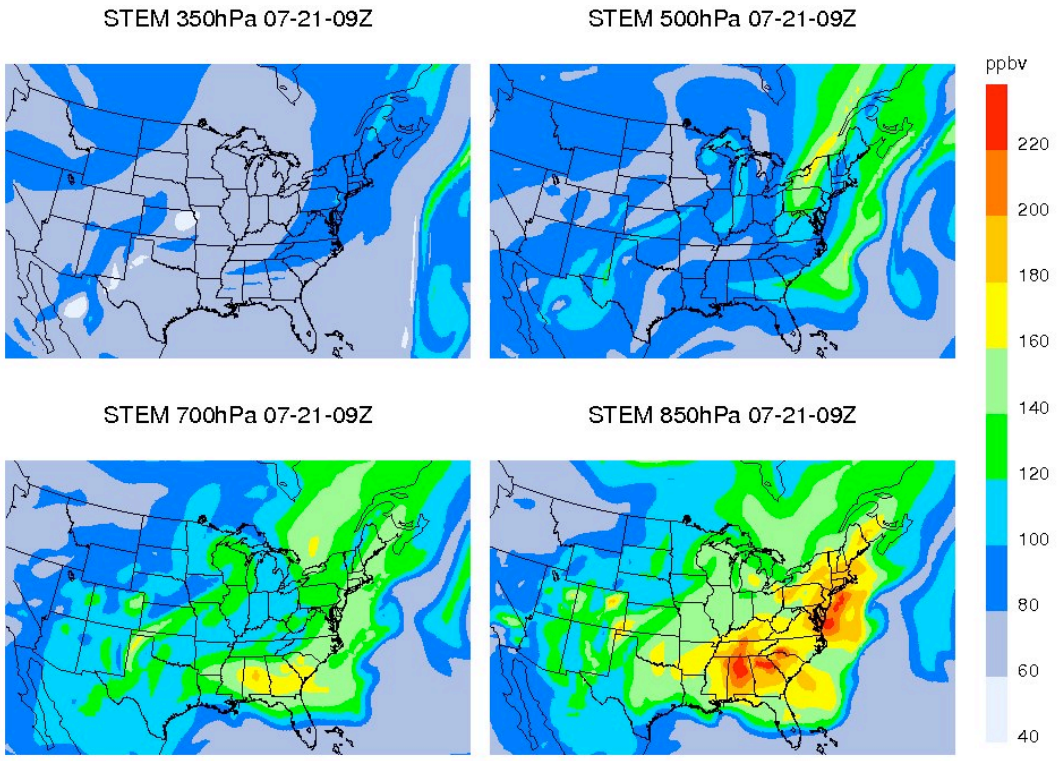

b)

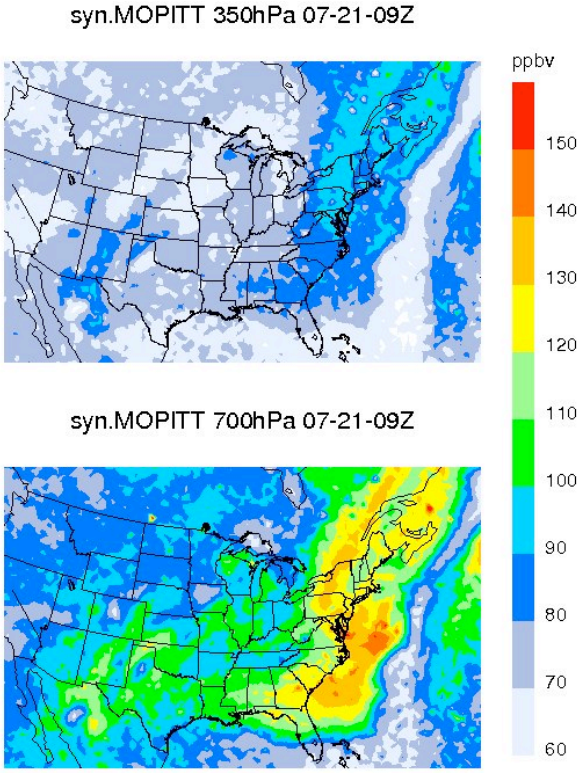

Figure 11. (a) STEM CO (ppbv) and (b) synthetic MOPITT CO (ppbv) for 21 July 2004 at 2100 UTC.

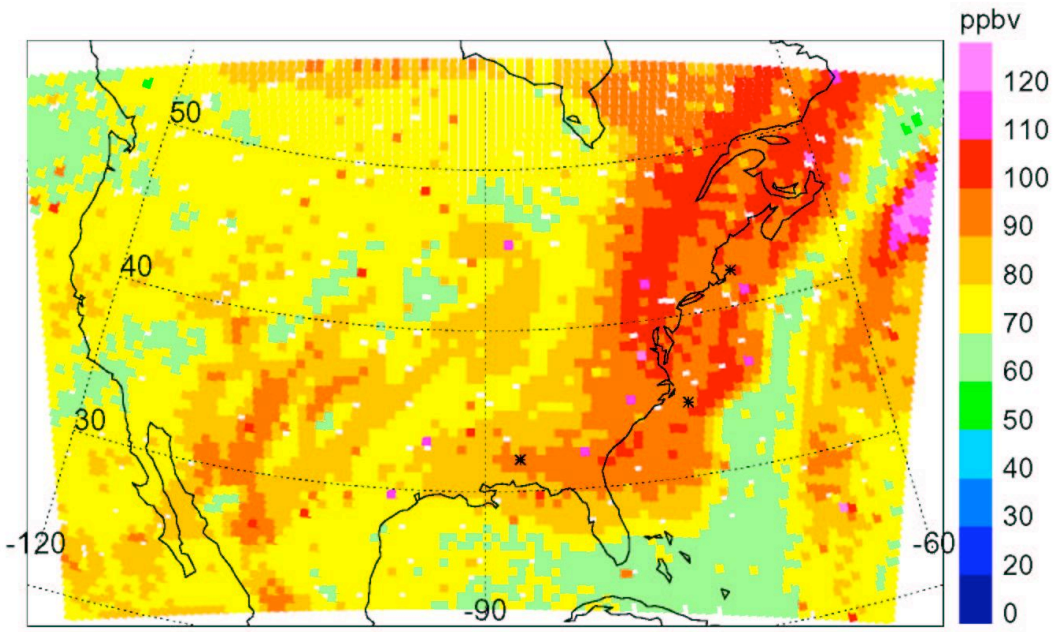

Figure 12. Map of MOPITT CO (ppbv) at 700 hPa indicating the locations of vertical profiles through the WCB examined on 21 July 2004. Vertical profiles are identified using black astericks.

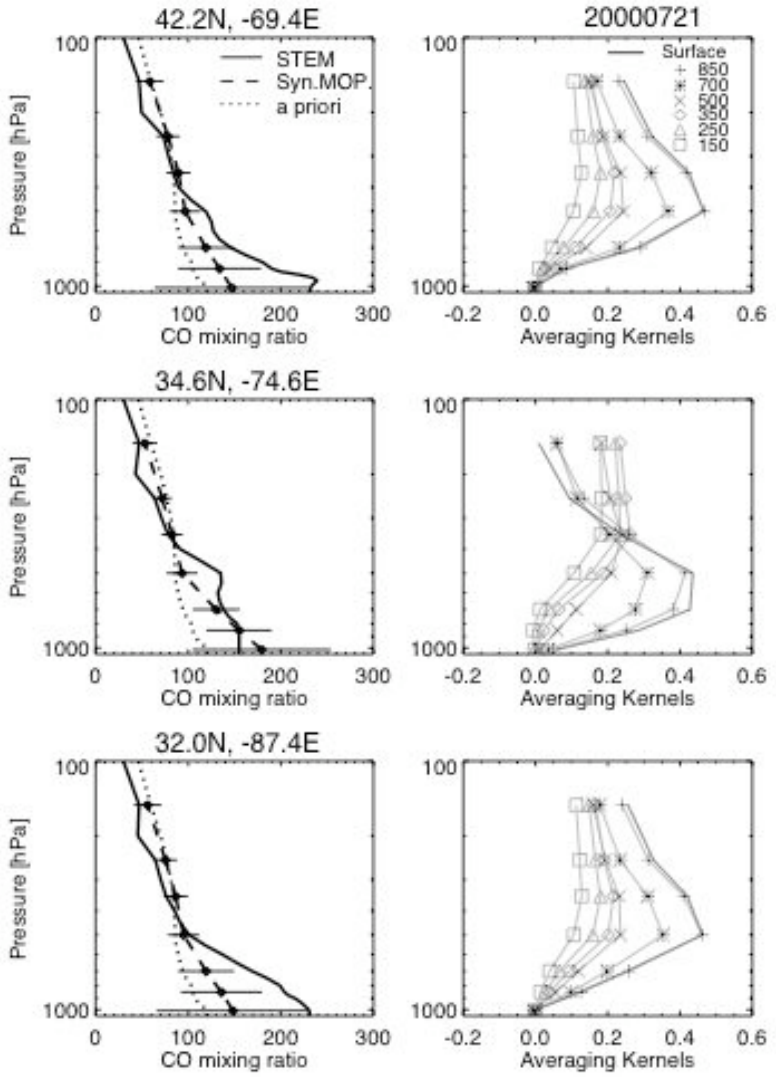

Figure 13. Vertical profiles of CO (ppbv) for 21 July 2004 at 0900 UTC at several locations in the WCB shown in Fig.11. The left panels show the STEM CO profile (solid line), the synthetic MOPITT CO profile (dashed line, with error bars), and the a priori CO profile (dashed, same in each). The right panels show the averaging kernels for each retrieval level (surface to 150 hPa).